2019

Biophysical analysis and NMR structural characterization of the binding between peptidomimetic drug CN2097 and scaffolding protein PSD-95

BOSTON UNIVERSITY

SCHOOL OF MEDICINE

Thesis

BIOPHYSICAL ANALYSIS AND NMR STRUCTURAL CHARACTERIZATION OF THE BINDING BETWEEN PEPTIDOMIMETIC DRUG CN2097 AND SCAFFOLDING PROTEIN PSD-95

by

TONY KEN HU

B.S., Boston College, 2017

Submitted in partial fulfillment of the

requirements for the degree of

Master of Science

2019

Approved by

First Reader

Carl Franzblau, Ph.D.
Professor of Biochemistry

Second Reader

John Marshall, Ph.D.
Professor of Medical Science
Brown University, School of Medicine

DEDICATION

I would like to dedicate this work to my friend Tiffany Yoyo Kwan, for being my motivation to strive for success.

ACKNOWLEDGMENTS

For the time, effort, and resources given to help write this work, I would like to acknowledge the following, in no particular order: Dr. Mandar Naik and Nandita Naik, Dr. John Marshall, Dr. Carl Franzblau, Dr. Gwyneth Offner, and Brown University's Structural Biology community and Department of Molecular Pharmacology, Physiology and Biotechnology.

BIOPHYSICAL ANALYSIS AND NMR STRUCTURAL CHARACTERIZATION OF THE BINDING BETWEEN PEPTIDOMIMETIC DRUG CN2097 AND SCAFFOLDING PROTEIN PSD-95

TONY KEN HU

ABSTRACT

Background: At the postsynaptic membrane of neurons there is a dense network of proteins called the postsynaptic density (PSD). One such protein is the postsynaptic density protein 95 (PSD-95), which functions as a molecular scaffold for forming protein complexes at the PSD. PSD-95 is composed of three PDZ domains, which studies have shown to be sequentially and structurally similar. Studies have shown that PSD-95 plays a role in regulating signaling of glutamatergic neurons, as well as the induction of long-term potentiation through an association with TrkB receptors. PSD-95 may be a promising target for treatment of a number of neurological disorders such as depression, epilepsy, and cognitive dysfunction. The cyclic peptidomimetic drug CN2097 was designed based on the PDZ-binding motif of the CRIPT protein that binds to PDZ3. While CN2097 has been shown to affect the binding of PSD-95 to different synaptic proteins, no NMR studies have been performed to characterize the binding of CN2097 to PDZ3. Furthermore, few studies have characterized the inter-domain interactions between PDZ domains or whether the binding of calmodulin (CaM) to the N-terminal region of PSD-95 has any effect on the binding between the PDZ domains and CN2097.

Objective: To use isothermal titration calorimetry and nuclear magnetic resonance spectroscopy to analyze and characterize how CN2097 binds to PDZ domains and whether inter-domain interactions exist between PDZ domains.

Methods: The gene sequences for the PDZ domains were inserted into the pET28a(+) vector by subcloning. *E. coli* bacteria were then transformed with the different PDZ plasmids. The bacterial cells were grown and induced to express the proteins of interest, followed by lysis and purification using affinity chromatography and fast protein liquid chromatography (FPLC). Isothermal titration calorimetry (ITC) was used to measure the dissociation constant and thermodynamic binding parameters between the peptidomimetic drug CN2097 and each isolated PDZ domain. Nuclear magnetic resonance (NMR) spectroscopy was used to study how CN2097 binds to PDZ1 and PDZ3, and how the PDZ domains interact with each other.

Results: The ITC data showed the dissociation constant between CN2097 and PDZ3 to be 5.12 ± (1.65) μM, and that of PDZ2+3 to be 42.63 ± (6.11)μM. ITC data on other domains was inconclusive. The NMR data showed no interaction between N-terminal region and PDZ1, and between PDZ2 and PDZ3 but significant interaction was seen between PDZ1 and PDZ2, as well as between PDZ3 and the inter-domain linker connecting it to PDZ2. NMR data showed that CN2097 binding perturbs PDZ3 more strongly than PDZ1 and that CN2097 does not bind to PDZ1 in the presence of CaM. Significant NMR chemical shift perturbations are seen on the second α-helix, second β-sheet, and β2-β3 loop.

Conclusions: There are no significant contacts between the N-terminal α-helix and PDZ1. There is inter-domain conformational exchange and interaction between PDZ1 and PDZ2. PDZ3 interacts with the second inter-domain linker. CN2097 binds tighter to PDZ3 than to PDZ1, and does not bind to PDZ1 in the presence of CaM. The β2-β3 loop is a prime target for future development of CN2097.

TABLE OF CONTENTS

LIST OF TABLES

LIST OF FIGURES

LIST OF ABBREVIATIONS

AMPA .....α-amino-3-hydroxy-5-methyl-4-isoxazolepropionic acid

BDNF .....Brain-derived neurotrophic factor

CaM.....Calmodulin

FPLC .....Fast protein liquid chromatography

GST .....Glutathione S-transferase

His ..... Polyhistidine

HSQC .....Heteronuclear single-quantum coherence correlation spectroscopy

IMAC ..... Immobilized metal ion affinity chromatography

ITC ..... Isothermal titration calorimetry

LTP ..... Long-term potentiation

NMDA ..... N-methyl-D-aspartate

NMR ..... Nuclear magnetic resonance

NOESY ..... Nuclear Overhauser effect spectroscopy

PDZ .....PSD-95 Discs large Zona occludens

PMSF .....Phenylmethylsulfonyl fluoride

PSD .....Postsynaptic density

PSD-95 ..... Postsynaptic density protein 95

SAP-90 ..... Synapse associated protein-90

SEC .....Size-exclusion chromatography

SH3 .....Src homology 3

TOCSY .....Total correlation spectroscopy

TrkB ..... Tropomyosin-related kinase B

INTRODUCTION

Postsynaptic density protein 95 and PDZ domains

The postsynaptic density (PSD) is a dense network of proteins located at the postsynaptic membrane, which has a vast array of roles, from signaling pathways to regulating structural changes (Boeckers, 2006). One of the many PSD proteins is postsynaptic density protein-95 (PSD-95), also known as synapse associated protein-90 (SAP-90), which is a scaffolding protein that plays a role in the localization and clustering of synaptic proteins (Piserchio et al., 2004). The synaptic proteins that interact with PSD-95 play a role in synaptic plasticity, which is affected in a wide range of neurological and cognitive, such as Alzheimer's disease, autism, schizophrenia, and chronic pain (Bliss, Collingridge, & Morris, 2014).

PSD-95 consists of five domains: three PDZ domains (initialism of **P**SD-95, **D**rosophila disc large, and **Z**onula occludens-1), an Src 3 (SH3) domain, and a guanylate kinase-like domain (Kim & Sheng, 2004). In addition to these five domains, there are two calmodulin (CaM)-binding regions, one on the N-terminal region (Zhang et al., 2014), and one on the region connecting SH3 and the guanylate kinase-like domain, also known as the HOOK region (Paarmann, Spangenberg, Lavie, & Konrad, 2002). Nuclear magnetic resonance (NMR) studies have revealed that the two lobes of CaM bind to PSD-95 by collapsing around the helical structure of the N-terminus of PSD-95 (Zhang et al., 2014). Under basal conditions, PSD-95 cycles between palmitoylation and depalmitoylation with the postsynaptic membrane (Fukata et al., 2013; Zhang et al.,

2014). Upon binding, CaM masks residues C3 and C5 of PSD-95, preventing palmitoylation of PSD-95 and shifting the equilibrium towards depalmitoylation (Zhang et al., 2014). In addition to the N-terminal and HOOK regions, CaM has been shown to also bind the PDZ2 and SH3 domains, but not the PDZ3 and guanylate kinase domains (Paarmann et al., 2002; Zhang et al., 2014). It is unknown whether CaM binds to PDZ1. The binding of CaM to the various domains could have potential implications when studying PDZ-binding drugs, as the binding of CaM to the N-terminal helix, PDZ2, SH3, and/or PDZ1 (if it binds at all) may potentially interfere with any drug or ligand binding.

The PDZ domain is found in over 200 proteins and contains between 80-100 residues (Lee & Zheng, 2010; Ponting, 1997). The three PDZ domains of PSD-95 have been shown to be highly similar both sequentially and structurally, in that they share the have similar fold created by two α-helices and six β-strands (Piserchio et al., 2004). PDZ domains bind to the C-terminal region of proteins containing the sequence motif (Ser/Thr)-X-(Val/Ile/Leu)-COOH (X being any amino acid) and is characteristic of the rapid association and dissociation between ligand and receptor as found in cell receptor signaling (Piserchio et al., 2004). The binding cleft is located between the second β-strand and the second α-helix (Doyle et al., 1996). Despite their similarity, each PDZ domain has a different preference for binding partners, and the origin to their individual specificity is unknown. The loop between the second and third β-strands in PDZ1 and PDZ2 has been shown through NMR studies to be affected during ligand association (Piserchio et al., 2002; Tochio, Hung, Li, Bredt, & Zhang, 2000), which potentially may play a part in the binding mechanism and/or specificity. It is also unclear whether there

are any inter-domain interactions between the PDZ domains, such as, between the N-terminal CaM-binding helix and PDZ1, and between PDZ2 and PDZ3.

Biological role of PSD-95 protein

As mentioned above, PSD-95 plays a role in the localization and clustering of synaptic proteins. An example of this is the association of PSD-95 with receptors to activate different signaling pathways. PSD-95 is known to associate with kainate receptors, *N*-methyl-D-aspartate (NMDA) receptors, and tropomyosin-related kinase B (TrkB) receptors (Cao et al., 2013; Garcia et al., 1998; Sornarajah et al., 2008), as well as indirectly regulating α-amino-3-hydroxy-5-methyl-4-isoxazolepropionic acid (AMPA) receptor surface trafficking (Bats, Groc, & Choquet, 2007). However, the mechanisms of how PSD-95 regulates receptor targeting, clustering, and facilitation of signaling are not entirely understood.

Kainate receptors are known to play a role in epilepsy, autism, and schizophrenia (Lerma & Marques, 2013). When coexpressed in HEK293 cells, PSD-95 has been found to promote the clustering of the GluK2 (GRIK2, GluR6) kainate receptor (Garcia et al., 1998). Indeed, PSD-95 has been found to serve as a scaffold of kainate receptors at hippocampal mossy fiber synapses (Suzuki & Kamiya, 2016). The activation of kainate receptors with GluK1 (GRIK1, GluR5) subunits has been shown to trigger seizures, although they are not necessary for their generation (Fritsch, Reis, Gasior, Kaminski, & Rogawski, 2014). The mechanism of kainate receptor clustering and targeting is not fully

understood. However, kainate receptors and the role PSD-95 plays are both topics of interest in the development of therapeutic drugs for the treatment of epilepsy.

As for NMDA receptors, it has been discovered that the direct binding of PDZ1 and PDZ2 domains of PSD-95 to the NR2A- or NR2B-containing subunits of NMDA receptors reduces desensitization of neuronal and non-neuronal cells (Sornarajah et al., 2008). NMDA receptor desensitization may protect against excitotoxicity caused by Ca^{2+} influx under repeated glutamate insult (Sornarajah et al., 2008), which plays a role in the severity of ischemic brain damage from stroke in animals (Aarts et al., 2002). NMDA receptor antagonists seemingly are not viable as therapeutic targets (Davis et al., 2000; Fix et al., 1993), but targeting the PDZ domains of PSD-95 as a means to decrease its association with NMDA receptors may be a potential therapeutic option for minimizing ischemic brain damage.

PSD-95 has been shown to interact with stargazin, a regulatory protein that associates with and localizes AMPA receptors to the PSD (Bats et al., 2007). The ubiquitination of PSD-95 in response to the activation of NMDA receptors untethers AMPA receptors from the postsynaptic membrane, allowing for their endocytosis and removal from synaptic sites (Colledge et al., 2003), essentially downregulating AMPA receptor signaling. A study has shown that an AMPA receptor antagonist, perampanel, was effective as an adjunctive treatment for epileptic seizures (French et al., 2013), supporting the concept that AMPA receptors are critical in epileptic synchronization and in the generation of epileptic discharges in humans (Rogawski, 2013). As PSD-95 plays a

role in the localization of AMPA receptors to the PSD, it may be worthy of being a target for developing treatments for epilepsy as well.

It has been shown that PSD-95 association with TrkB receptor is critical for brain-derived neurotrophic factor (BDNF) TrkB signaling, which is known to induce and maintain long-term potentiation (LTP), a form of synaptic plasticity that is involved in cognitive function (Cao et al., 2013). A proposed possible role of PSD-95 in BDNF-derived TrkB signaling is that upon binding of BDNF to TrkB, PSD-95 is recruited to the receptor to facilitate downstream signaling (Cao et al., 2013). Following traumatic brain injury, BDNF is dysregulated (Marshall et al., 2017), and in neurological disorders such as Angelman syndrome, BDNF-derived TrkB signaling is impaired by the interference of elevated levels of activity-regulated cytoskeletal-associated protein (Arc; Cao et al., 2013). There has been development of a drug, CN2097, as a potential therapeutic that binds to the PDZ domains of PSD-95, decreasing its interaction with Arc (Cao et al., 2013).

There is a great deal about PSD-95 that is unknown. Kainate, AMPA, NMDA, and TrkB receptors are only a few of the known synaptic membrane proteins that PSD-95 interacts with; the extent of PSD-95 interactions with other synaptic proteins in the PSD remains unclear. Because of its involvement in a wide range of protein complexes at the postsynaptic membrane, any potential therapeutic agents targeting PSD-95 will require a wide range of experiments to decrease the amount and severity of any inadvertent side effects.

Peptidomimetic drug CN2097

As mentioned before, a ligand that binds to PSD-95 could be a potential therapeutic agent for epilepsy, reducing stroke-associated ischemic brain damage, and the mitigation of cognitive dysfunction. A cyclic peptide based on the C-terminal six residues of the CRIPT protein was designed to bind to PDZ3 of PSD-95 (Li, Saro, & Spaller, 2004). The CRIPT protein is a linear peptide that has been structurally characterized to bind to PDZ3 (Niethammer 1998), the primary binding residues being the C-terminal (P_0) and the antepenultimate (P_{-2}) residues (Li et al., 2004). A bridging approach was used when designing the peptide, creating a β-Ala lactam linker in order to overcome the unfavorable distortion on the peptide backbone by way of covalently connecting the P_{-1} and P_{-3} residues so as to exhibit overall conformational diversity (Li et al., 2004).

Aside from binding to PDZ3, another study has shown that the cyclic peptide also binds to PDZ1 of PSD-95 (Piserchio et al., 2004). The sequence motif that binds to the PDZ domains is known and was previously described above. Piserchio et al. (2004) performed NMR spectroscopy on the titration of PDZ1 with the cyclic peptide and showed the amino acid residues that are affected during binding (**Figure 1**). However, no such experiment was conducted on PDZ3, which was the target when the cyclic peptide was designed. LeBlanc et al. (2010) designed and synthesized the drug CN2097 by adding a polyarginine moiety to the N-terminus of the cyclic peptide, thus improving the permeability of the cyclic peptide across cellular membranes.

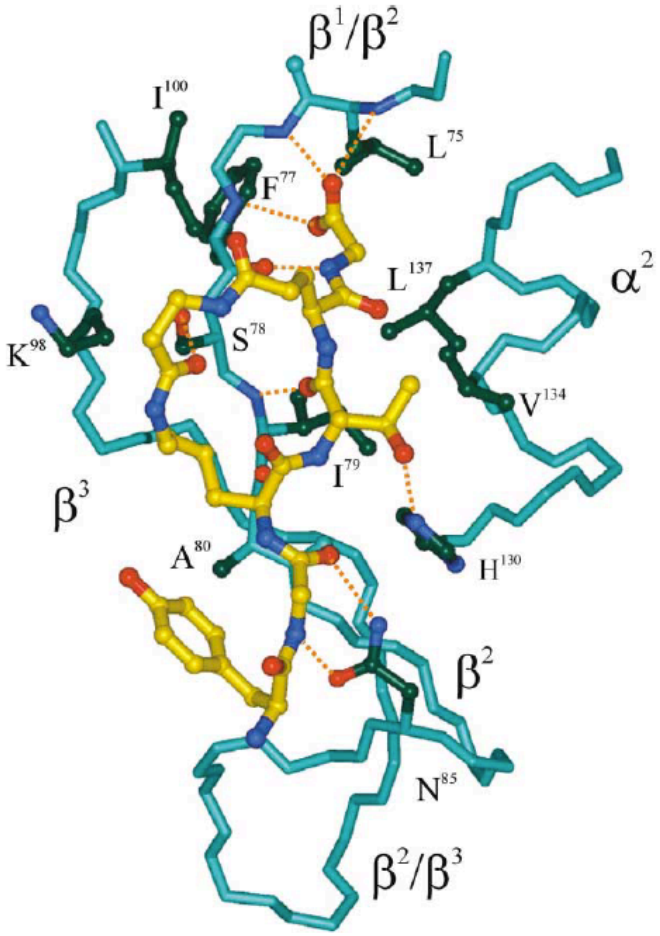

Figure 1: Binding of CN2097 to PDZ1. The specific residues involved in the binding of CN2097 to PDZ1 are labeled and depicted here in dark green (Piserchio et al., 2004).

As mentioned, it is unknown whether CaM binds to PDZ1 or whether CaM interferes with the binding of CN2097 to the PDZ domains. Previously, a concentration of 400μM CRIPT peptide was shown to enhance the binding between PSD-95 and CaM (Fukunaga, Matsubara, Nagai, & Miyazawa, 2005). Although the CRIPT peptide only binds PDZ3 and the design of CN2097 was based on CRIPT, it is unknown if CN2097 elicits a similar effect.

Isothermal titration calorimetry and its use

Isothermal titration calorimetry (ITC) is a technique that is used to study protein-protein, protein-small molecule, protein-DNA/RNA interactions, enzyme kinetics, as well as protein folding and unfolding (Liang, 2008). It is the only technique that directly determines the thermodynamic parameters of a reaction: the enthalpy change (ΔH), the change in Gibbs free energy (ΔG), the entropy change (ΔS), and the heat capacity change in the process (ΔC_p) (Velazquez-Campoy, Leavitt, & Freire, 2004). When studying protein-protein interactions, the binding partners can be different proteins or even the same protein (i.e., homodimer). Regardless of the type of interaction or binding partners involved, the underlying principles of ITC are the same.

When a ligand and a protein bind, there is a change in the enthalpy, free energy, and entropy that can be measured through an increase or decrease in temperature. During an ITC experiment, stepwise injections of the ligand are added into a calorimetric cell via a syringe (Velazquez-Campoy et al., 2004). The cell is maintained at a constant temperature. As the ligand is injected and binds to the protein, small changes in temperature are measured as different changes in energy supplied to the cell. The association constant K_a, the stoichiometric number N, and the change in enthalpy ΔH can all be determined based on the heat changes, cell concentrations, and syringe concentrations. From those values, ΔG, ΔS, ΔC_p, and the dissociation constant K_d can also be estimated. In addition to the experiment of adding the ligand to the protein, a blank experiment of adding ligand to buffer is required to account for the contribution of the enthalpy of dilution.

When designing the cyclic peptide portion of CN2097, ITC was used to measure the dissociation constant between the cyclic peptide and PDZ3 (Li et al., 2004), which indicated whether or not there was binding between the peptide and PDZ3. ITC is used in this study to characterize drug CN2097 binding to all three PDZ domains.

Biomolecular NMR spectroscopy and its use

While ITC is useful to observe the binding of a ligand to a protein, it is rather crude when compared to NMR spectroscopy in terms of determining whether binding happens or not. NMR spectroscopy is the technique for determining the structure of a molecule, in this case the protein and the peptidomimetic drug. NMR spectroscopy works by detecting the electromagnetic waves that are generated by nuclei when they are subjected to a magnetic field, and a weaker, oscillating magnetic field (Doucleff, Hatcher-Skeers, & Crane, 2011). Different nuclei are affected invariably by the magnetic field, as the surrounding electrons tend to lower or negate the effects of the external magnetic field. Neighboring atoms, depending on their electronegativity, will therefore have varying effects on the signals through J-coupling if covalently bonded, or dipole-dipole coupling if less than 5Å apart (Doucleff et al., 2011). The effects of J-coupling can be analyzed using heteronuclear single-quantum coherence correlation spectroscopy (HSQC) and the effects of dipole-dipole coupling can be analyzed using nuclear Overhauser effect spectroscopy (NOESY).

For biological NMR spectroscopy, signals produced by hydrogen, nitrogen, and carbon atoms are most useful in characterizing the structures of proteins. However, only

nuclei with spins of ½ (e.g., ^{1}H, ^{13}C, and ^{15}N) generate signals that can be easily analyzed. Nuclei with a spin of zero (e.g., ^{12}C) generate no signals, and nuclei with spins greater than ½ (e.g., ^{14}N) generate signals that are too short, dampened, and difficult to detect due to their electric quadrupolar moment (Doucleff et al., 2011). Obtaining just the 1D- ^{1}H spectrum of protein samples is not very informative due to signal overlap. Instead, obtaining a 2D- ^{1}H-^{15}N HSQC spectrum shows protons that are covalently bonded to nitrogen atoms, while an 2D- ^{1}H-^{13}C HSQC spectrum shows protons that are covalently bonded to carbon atoms (Doucleff et al., 2011). Because of this, when expressing proteins for NMR, M9 media, which contains ^{15}N-labeled ammonium chloride, is used to grow cells in conjunction with the optional addition of ^{13}C-labeled glucose. When both are used, triple resonance experiments can be conducted to provide assignments of individual residues in a protein. Two such triple resonance experiments are 3D- HNCA and 3D- HNCO, both of which were used in this study. HNCA correlates the amide ^{1}H and ^{15}N shifts of a residue with the Cα shifts of a residue as well as the preceding residue, while HNCO correlates the amide shifts of a residue with the carbonyl carbon shift of the preceding residue (Kay, Ikura, Tschudin, & Bax, 1990).

In this study, 2D- HSQC was used to structurally characterize the binding between CN2097 and the isolated PDZ domains as well as to characterize inter-domain interactions between PDZ domains. The HSQC experiments served to supplement the ITC data acquired on the binding between CN2097 and the PDZ domains and provided residue-specific information about the binding interface. The spectrum can be analyzed to show which amino acids are affected upon binding. Each amino acid generates a distinct

signal that would change upon binding. The ^{1}H-^{15}N HSQC spectra would change if CN2097 bound to a PDZ domain or if inter-domain interactions are present. Normally, performing a titration of protein with a ligand would show how each residue is affected during binding and can be used to calculate the apparent dissociation constant (EC50), but this was not conducted as we have more accurate information from the ITC experiment. HNCA and HNCO experiments were performed on the PDZ3/CN2097 complex in addition to 2D total correlation spectroscopy (TOCSY) being performed on CN2097. The purpose of these experiments was to obtain backbone and side-chain assignments for the PDZ3/CN2097 complex. The assignments would eventually allow for calculating the 3D structure of the PDZ3/CN2097 complex, which would be immensely helpful for the future development of the drug.

MATERIALS AND METHODS

Cells, plasmids, and peptidomimetic drug

BL21 (DE3) competent *E. coli* cells were used for the protein expression necessary for this experiment. pGEX-4T1 PDZ domain plasmids and the peptidomimetic drug CN2097 were provided by Dr. John Marshall of the Department of Molecular Pharmacology, Physiology and Biotechnology at Brown University. These plasmids contained the gene for one the following PDZ domains of PSD-95: PDZ1 with the N-terminal CaM-binding region (PDZ1long), PDZ2, PDZ3, the combined domains of PDZ1 and PDZ2 (PDZ1+2), and the combined domains of PDZ2 and PDZ3 (PDZ2+3). The residue numbers of PSD-95 that each recombinant protein contained can be seen in **Figure 2**. PDZ1long extended from residues 1-151, PDZ1 from residues 65-151, PDZ2 from 160-246, PDZ3 from 313-393, PDZ1+2 from 65-246, PDZ2+3 from 160-393, and PDZ1+2+3 from 1-393. In addition, a pET11d-PDZ1 plasmid was used in this study. Calmodulin plasmid was obtained from Addgene.

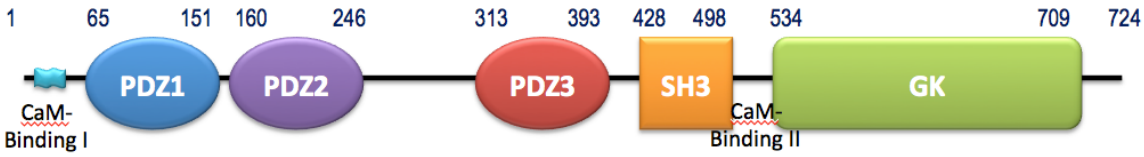

Figure 2: Domain Architecture of PSD-95. The residue numbers of the different PDZ domains is shown here, in addition to all the domains and regions of PSD-95. The linkers and domains are not shown to scale.

Subcloning PDZ genes into pET28a(+) vector

BL21 (DE3) cells were initially transformed with the GST fusion plasmids with the intention of expressing the PDZ domains with a N-terminal glutathione S-transferase (GST) tag and thrombin-cutting site. However, the thrombin protease failed to fully cleave the GST tag from the PDZ domains and lead to degradation of the PDZ protein. The gene corresponding to the domains in each of these plasmids were amplified by PCR and subcloned into the pET-28a(+) recombinant vector. The restriction enzymes EcoRI and SalI were used for PDZ1, PDZ3, and PDZ2+3. The restriction enzymes EcoRI and XhoI were used for PDZ2 and PDZ1+2. The success of creating new plasmid vectors was determined by DNA sequencing. In addition a plasmid was created, containing all three PDZ domains as well as the N-terminal CaM-binding region (PDZ1+2+3).

Expressing PDZ domains and CaM

A 1μL aliquot of each plasmid was used to transform ~50μL of BL21 cells. The cells were then transferred in 25mL LB media starter cultures and incubated at 37˚C, 300rpm overnight. The starter cultures were then added to 800mL LB media and incubated at 37˚C, 200rpm until the OD_{600} reached 0.4-0.8, at which point isopropyl β-D-1-thiogalactopyranoside (IPTG) was added for a working concentration of 0.5mM, and further incubated for 3 to 4 hours. A similar protocol was followed for expressing the ^{15}N-labeled and $^{15}N/^{13}C$-labeled protein, with the only exception being the use of M9 media supplemented with $^{15}NH_4Cl$ or $^{15}NH_4Cl/^{13}C$-glucose instead of LB media.

Protein purification

For the PDZ domains and CaM, the 800mL cell cultures were centrifuged at 4000rpm, 4˚C until a cell pellet formed, at which point the media was discarded and the pellet re-suspended in high salt buffer (pH=8.0, 1M NaCl, 50mM KH_2PO_4). Cells were lysed by adding Triton X-100 (1μL/mL of cell suspension) and by sonication. Phenylmethylsulfonyl fluoride (PMSF) in isopropanol was added at a final concentration of 100-150μM to inhibit protein breakdown by bacterial serine proteases. The cell lysate suspension was centrifuged at 14,000rpm, 4˚C until a pellet formed.

Each PDZ domain contained a polyhistidine (His) tag, and therefore the cell lysate for those proteins was purified by immobilized metal ion affinity chromatography (IMAC). The cell lysate of the PDZ domains were passed on fast protein liquid chromatography (FPLC) with a HisPrep™ Fast Flow 16/10 column. All proteins in IMAC were eluted using 50mM potassium phosphate buffer with 100mM NaCl and 250mM imidazole (pH 7.5). The presence of the correct protein was determined by polyacrylamide gel electrophoresis. All protein samples were then concentrated to a total volume of ~5mL. All proteins needed to be purified by size-exclusion chromatography (SEC) to eliminate the presence of imidazole, and therefore were passed on FPLC with a HiLoad® 16/600 Superdex® 75 column using 50mM potassium phosphate buffer with 100mM NaCl (pH=7.5). All protein samples were then concentrated to ≤2mL. The purity of the protein was also checked by polyacrylamide gel electrophoresis.

A similar protocol was followed for purifying CaM. Since CaM was expressed with a GST-tag, it was first purified on FPLC with a GSTPrep™ Fast Flow 16/10

column. Thrombin was used to cleave the GST-tag from CaM before being purified by SEC.

ITC experiments and analysis

The concentration of each purified protein sample was determined by measuring the UV absorption of each sample at 280nm using a spectrophotometer and calculating the concentration based on Beer's Law. Experiments were performed with an iTC200 titration microcalorimeter (Microcal, Inc.). The drug CN2097 was weighed out and dissolved in the same buffer used during SEC, for a concentration of 1mM. All ITC experiments were conducted at 25˚C in 50mM potassium buffer with 100mM NaCl (pH=7.5) and all solutions were degassed. The typical titration had the ligand (~1mM) injected into isolated PDZ domains (100μM), with the exception of three titrations of PDZ2+3, which were conducted with a protein concentration of 50μM. ITC experiments were conducted on PDZ1long, PDZ1, PDZ2, PDZ3, PDZ1+2, and PDZ2+3. The heat of dilution was measured with a blank titration of the ligand into the buffer, and subtracted from each titration experiment. All ITC data was analyzed using Origin software (*version 5.0*, Microcal).

NMR spectroscopy and residue assignments

All NMR spectra were collected at 20˚C using a Bruker NEO 600MHz spectrometer. ^{1}H-^{15}N HSQC experiments were performed on the following: PDZ1long, PDZ1, PDZ2, PDZ3, PDZ1+2, PDZ2+3, PDZ1+2+3, PDZ1/CN2097 complex,

PDZ3/CN2097 complex, PDZ1long/CaM complex, and PDZ1long/CaM/CN2097 complex. In addition to HSQC experiments, 3D- HNCA and 3D HNCO experiments were both performed on PDZ3 and PDZ3/CN2097 complex and a 2D- TOCSY experiment was performed on CN2097. The final concentration ratio of CaM to PDZ1long was 1:1, and the final concentration ratio of the PDZ domain complex to CN2097 was also 1:1. NMRFAM-Sparky was used to analyze the 3D spectra to assign amino acid residues.

The NMR experiments of the PDZ1long-CaM complex and the PDZ1long-CaM complex with CN2097 were conducted with a 500μL solution containing 74μM 15N labeled PDZ1long protein, 74μM unlabeled CaM protein, and 74μM CN2097 in 50mM potassium phosphate buffer, 100mM NaCl (pH 7.5), and 10% (v/v) D2O. Other NMR experiments were conducted similarly with protein concentrations ~100μM and the protein to CN2097 ratios was 1:1.

RESULTS

ITC results of CN2097 binding to PDZ domains

The ITC experiments were inconclusive in determining binding parameters for PDZ1long, PDZ1, PDZ2, and PDZ1+2. The generation of heat from multiple experiments involving PDZ1long, PDZ1, PDZ2, and PDZ1+2 was too little to reliably determine binding parameters. ITC data was insufficient to determine how the N-terminal CaM-binding region affects the binding of CN2097 to PDZ1, as well as how PDZ2 affects the binding of CN2097 to PDZ1.

The dissociation constant of PDZ3 was determined to be 5.12 ± (1.65) μM. The dissociation constant of PDZ2+3 was determined to be 42.63 ± (6.11) μM. Table 1 displays the values of the other binding parameters for PDZ3 and PDZ2+3. The ITC data of PDZ3 and PDZ2+3 that was used in determining their thermodynamic parameters can be seen in **Figure 3** and **Figure 4**. The lower dissociation constant of PDZ3 compared to PDZ2+3 indicates that CN2097 binds to isolated PDZ3 more tightly.

Table 1. Thermodynamic Parameters of the Binding of CN2097 to PDZ domains from PSD-95[A]

PDZ Domain	K_d (μM)	ΔG (kcal/mol)	ΔH (kcal/mol)	TΔS (kcal/mol)
PDZ1long[B]	–	–	–	–
PDZ1[B]	–	–	–	–
PDZ2[B]	–	–	–	–
PDZ3	5.12 ± (1.65)	-3.63 ± (0.17)	-3.30 ± (0.20)	0.33 ± (0.03)
PDZ1+2[B]	–	–	–	–
PDZ2+3	42.63 ± (6.11)	-6.55 ± (0.88)	-6.61 ± (0.97)	-0.05 ± (0.09)

[A] Values are the average of two independent experiments performed at 25˚C.
[B] The generation of heat for multiple experiments was too small to reliably determine binding parameters.

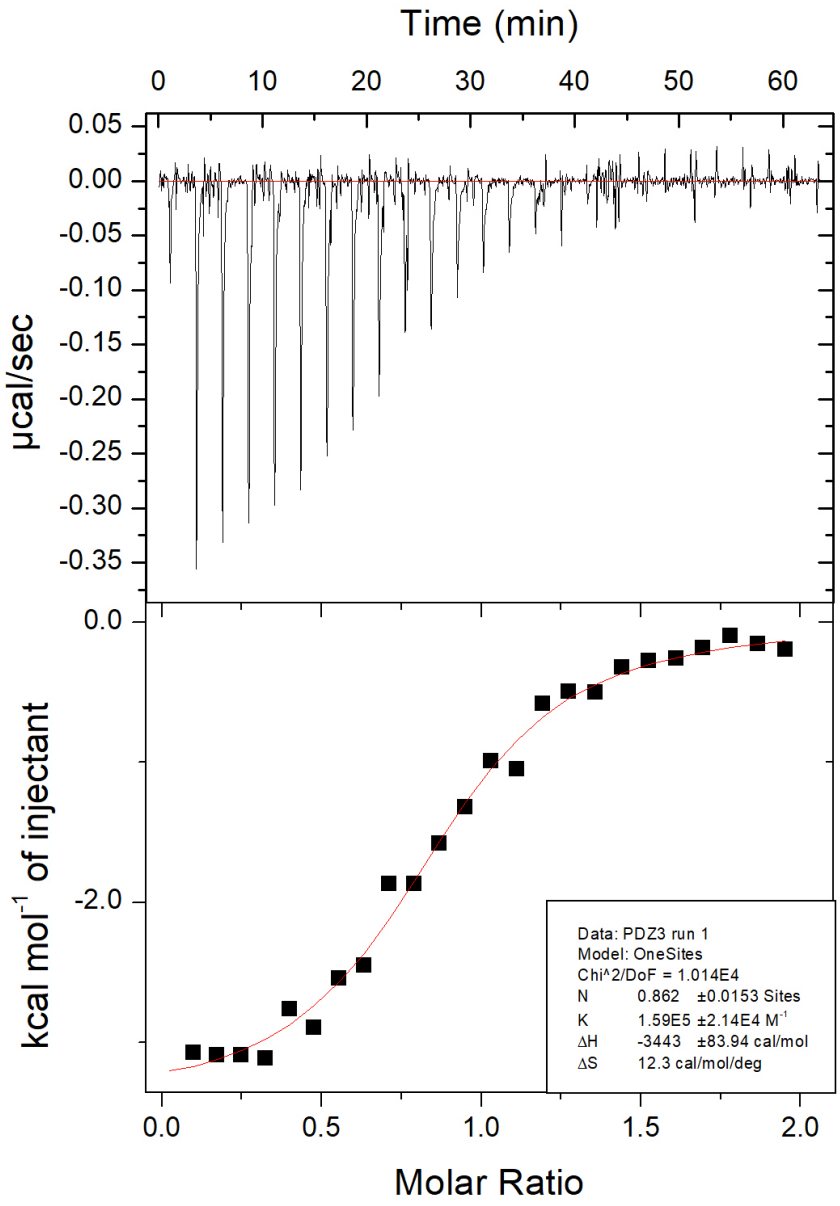

Figure 3. ITC thermogram of the titration of 100µM PDZ3 with 1mM CN2097.

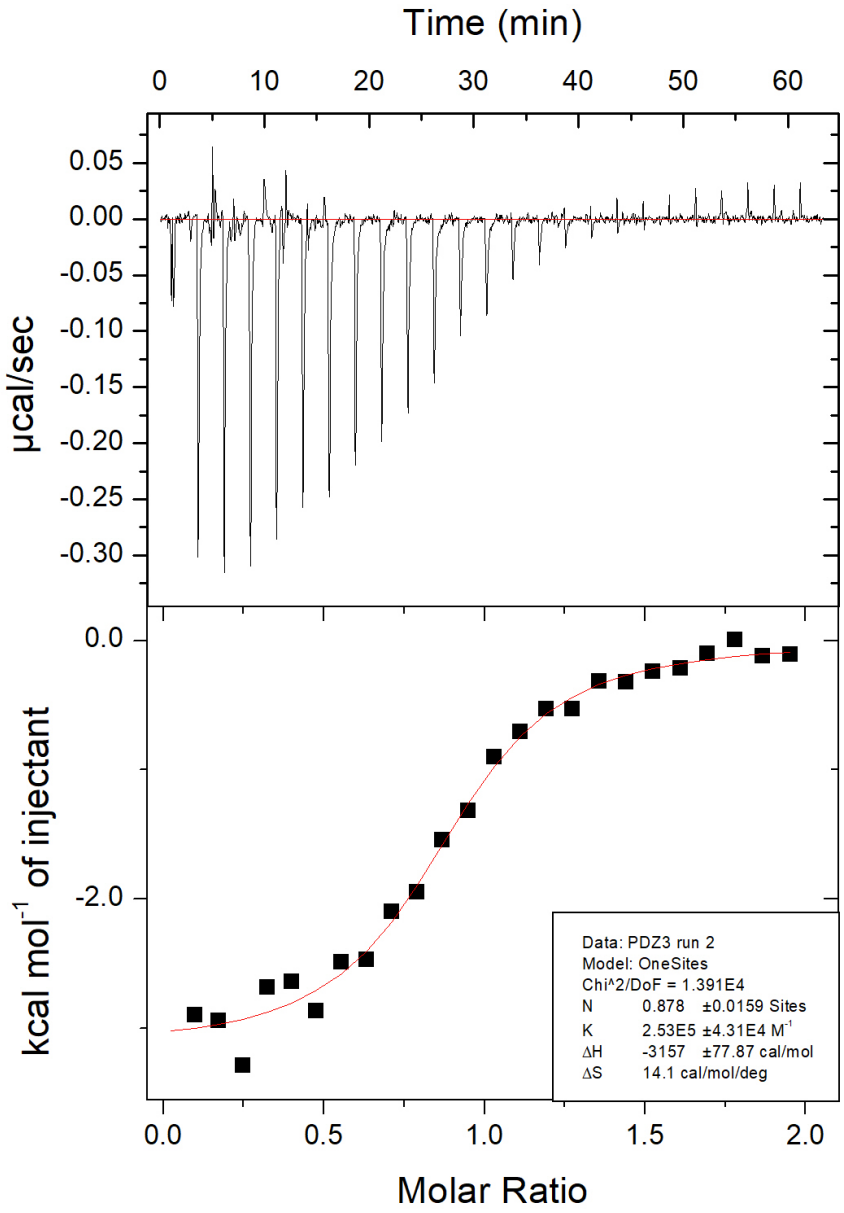

Figure 3 continued. ITC thermogram of the titration of 100µM PDZ3 with 1mM CN2097.

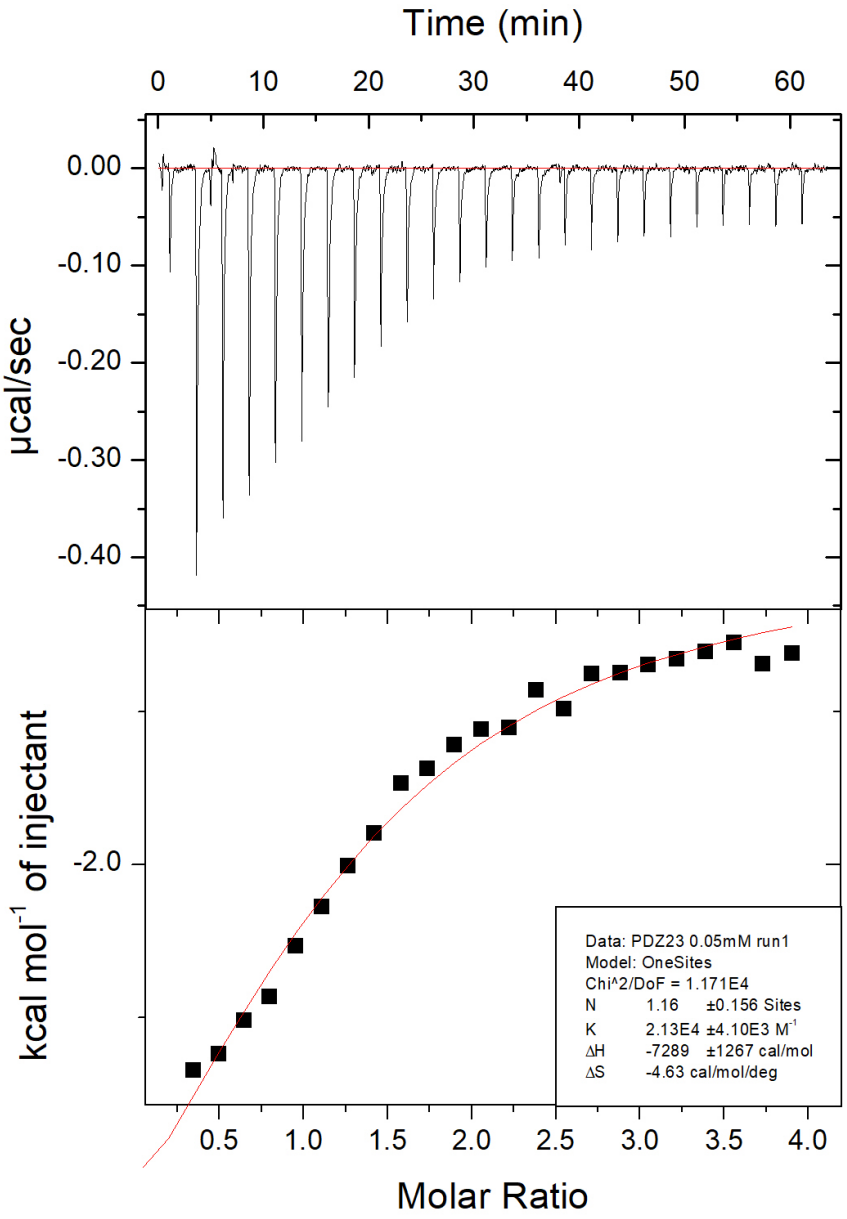

Figure 4. ITC thermogram of the titration of 50µM PDZ2+3 with 1mM CN2097.

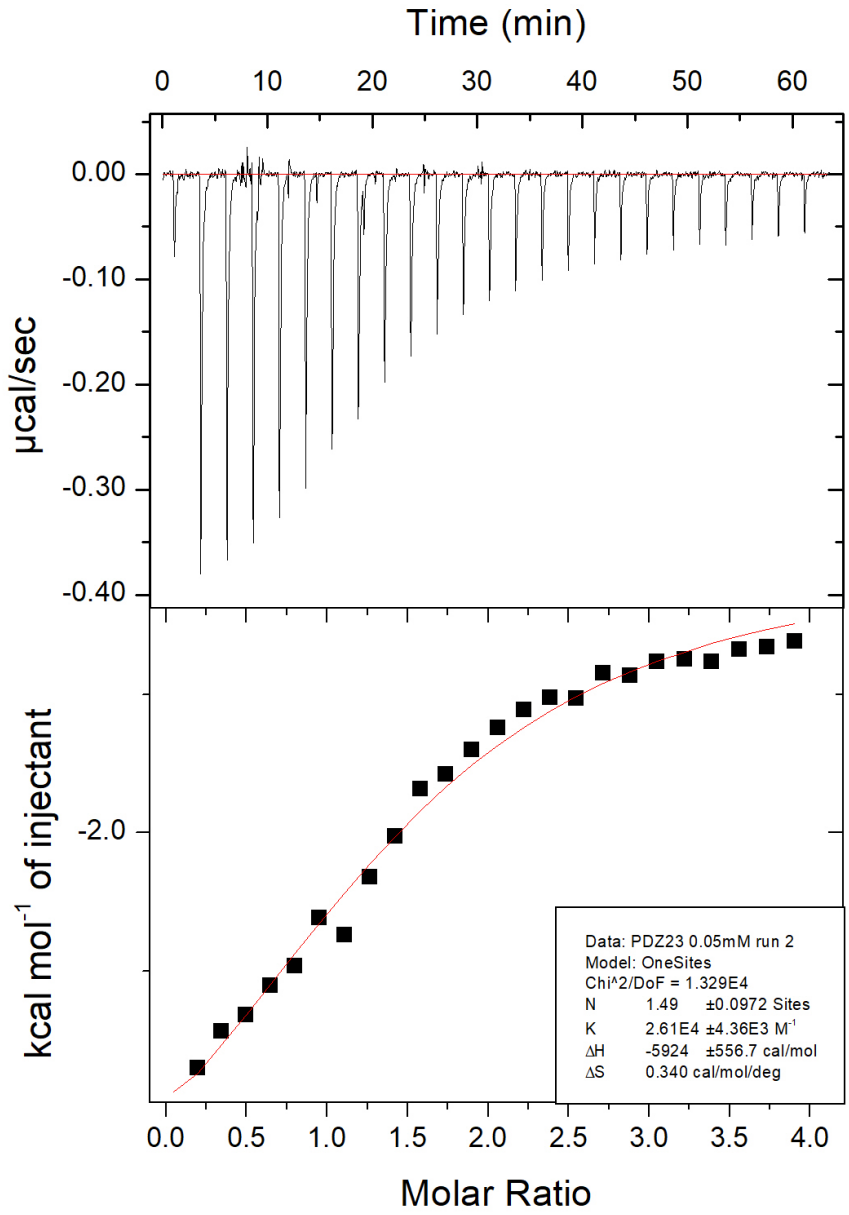

Figure 4 continued. ITC figures of the titration of 50µM PDZ2+3 with 1mM CN2097.

NMR spectroscopy of PDZ inter-domain interactions

Residue specific snapshots of isolated PDZ domain structures were obtained by NMR ^{15}N-HSQC spectrum (**Figure 5**). The resonance peaks of PDZ1, PDZ2, and PDZ3 are monodispersed and well resolved, indicating that each domain is well folded in

solution. Based on the different HSQC spectrum of each isolated domain, it can be determined that the domains are considerably different from each other.

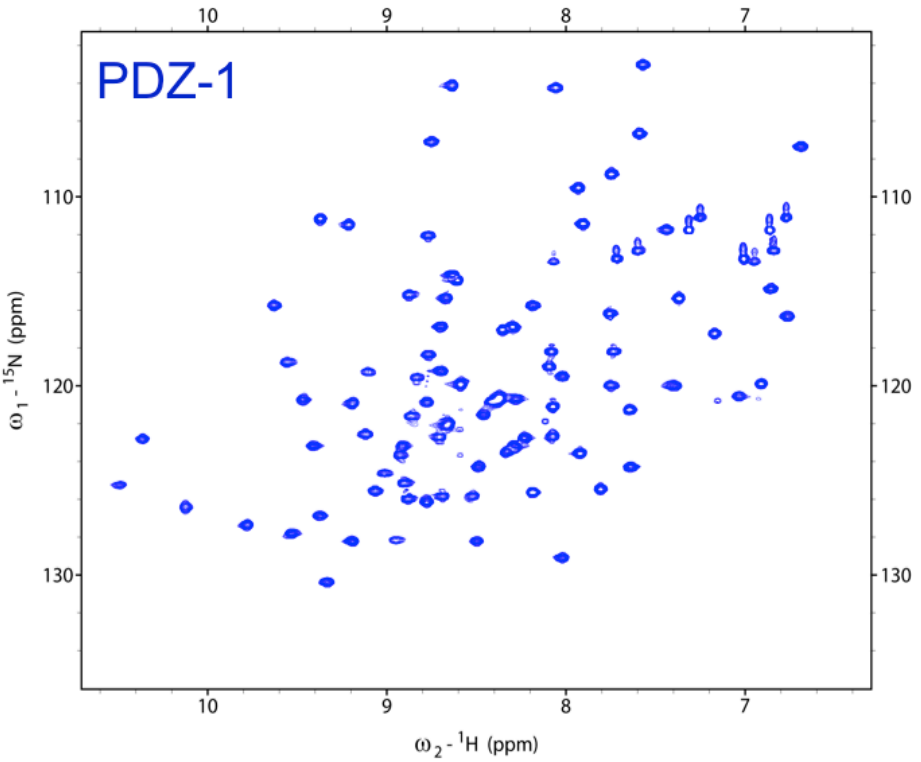

Figure 5: ^{15}N-HSQC spectrum of PSD-95 isolated PDZ domains. Each peak denotes a backbone amide of a non-proline residue or side chains of Asn, Arg, Gln, and Trp.

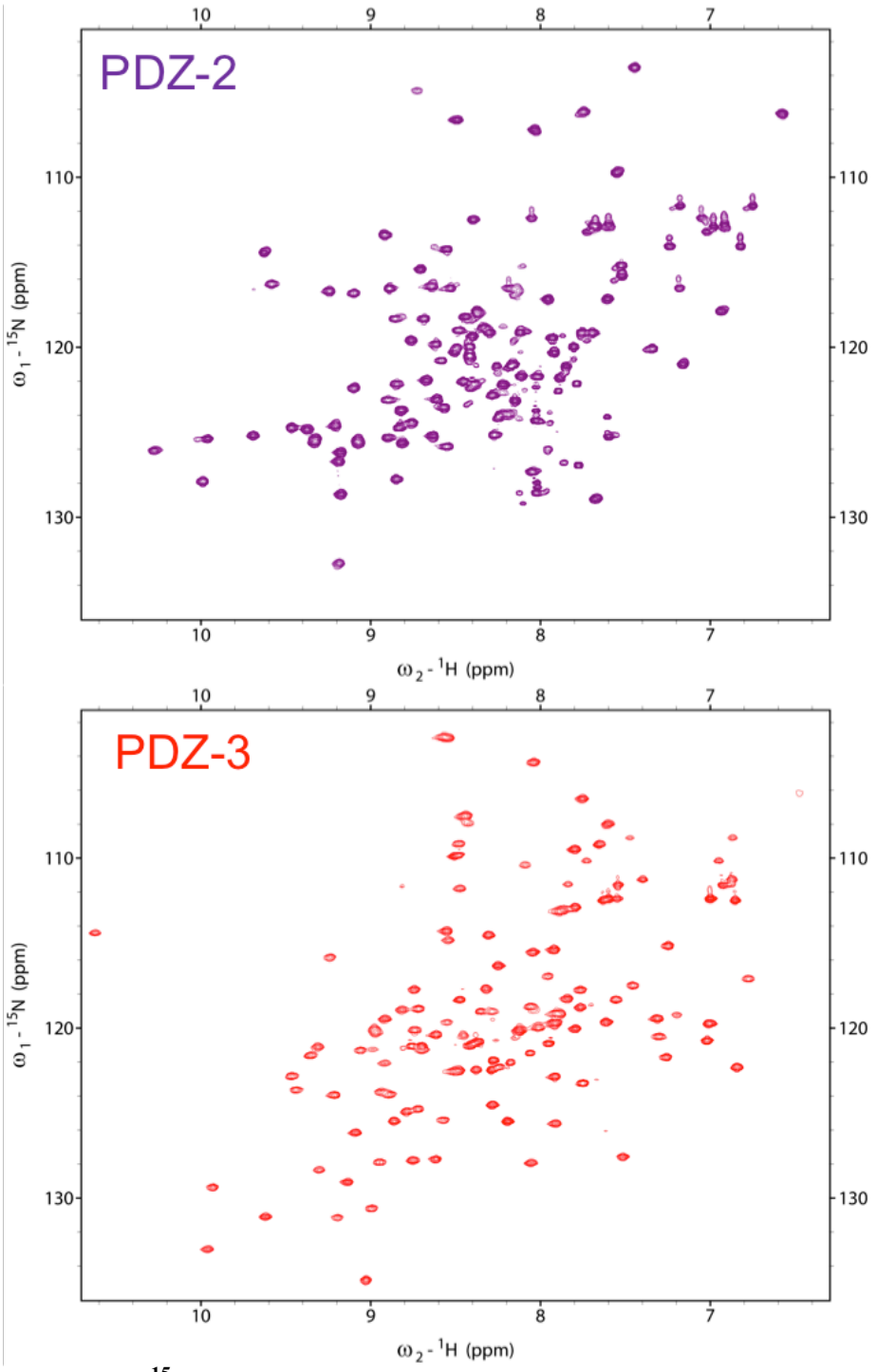

Figure 5 continued: ^{15}N-HSQC fingerprinting of PSD-95 isolated PDZ domains. Each peak denotes a backbone amide of a non-proline residue or side chains of Asn, Arg, Gln, and Trp.

A residue specific snapshot of PDZ1long structure was obtained by NMR ^{15}N-HSQC spectrum (**Figure 6**). The resonance peaks of PDZ1long are monodispersed and well resolved, indicating that it is well folded in solution. Comparison of the HSQC of PDZ1long and PDZ1 by overlaying the two spectra shows that there are no significant perturbations in the PDZ1 peaks (**Figure 7**). There are additional peaks and minor differences that can be attributed to the addition of an N-terminal α-helix in PDZ1long, which is to be expected. The lack of significant perturbations indicates that the N-terminal CaM-binding α-helix does not interact with PDZ1.

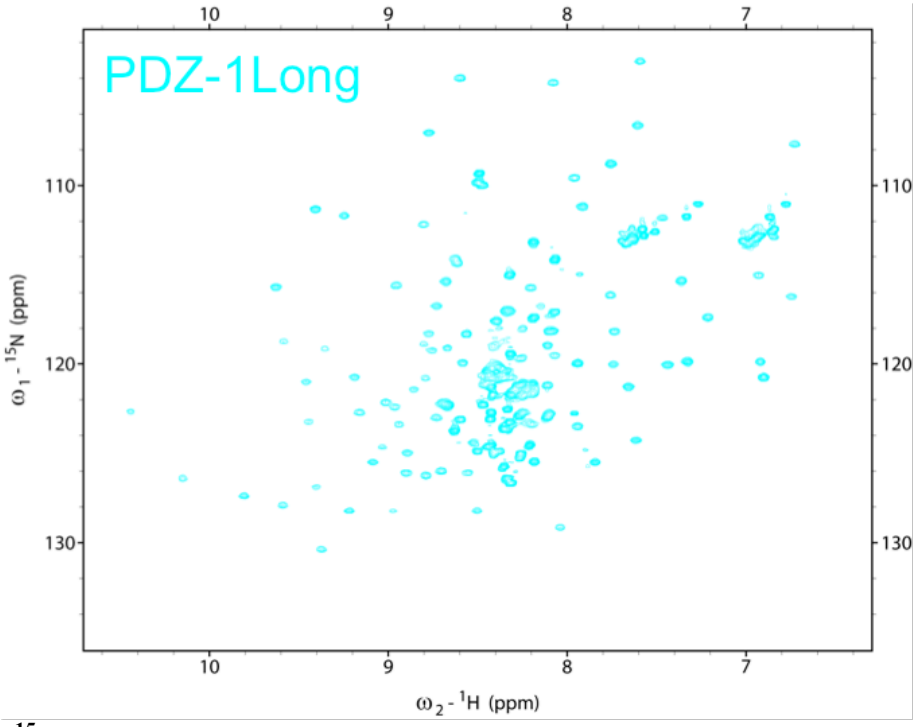

Figure 6: ^{15}N-HSQC of PDZ1long. Each peak denotes a backbone amide of a non-proline residue or side chains of Asn, Arg, Gln, and Trp.

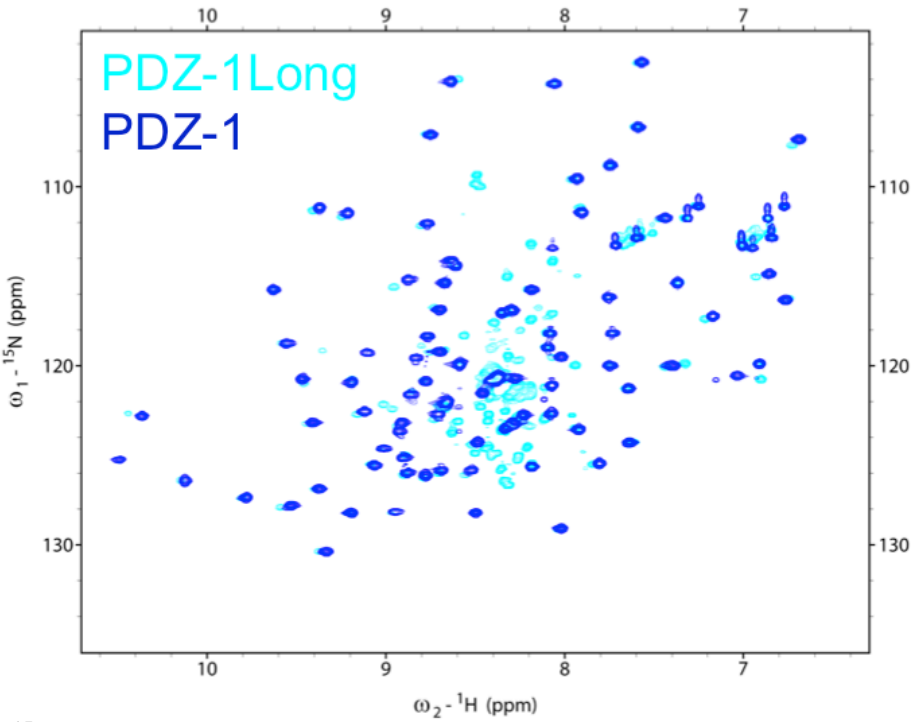

Figure 7: ^{15}N-HSQC overlay of PDZ1 on PDZ1long. Each peak denotes a backbone amide of a non-proline residue or side chains of Asn, Arg, Gln, and Trp. No significant perturbations in PDZ1long indicate no significant contacts exist between the N-terminal α-helix and the PDZ1 domain.

A residue specific snapshot of PDZ1+2 structure was obtained by NMR ^{15}N-HSQC spectrum (**Figure 8**). Comparison of the HSQC of PDZ1, PDZ2, and PDZ1+2 by overlaying the three shows that resonance peaks of PDZ1+2 have of uneven intensity (**Figure 9**). This indicates the presence of inter-domain conformational exchange and interaction between PDZ1 and PDZ2 domains.

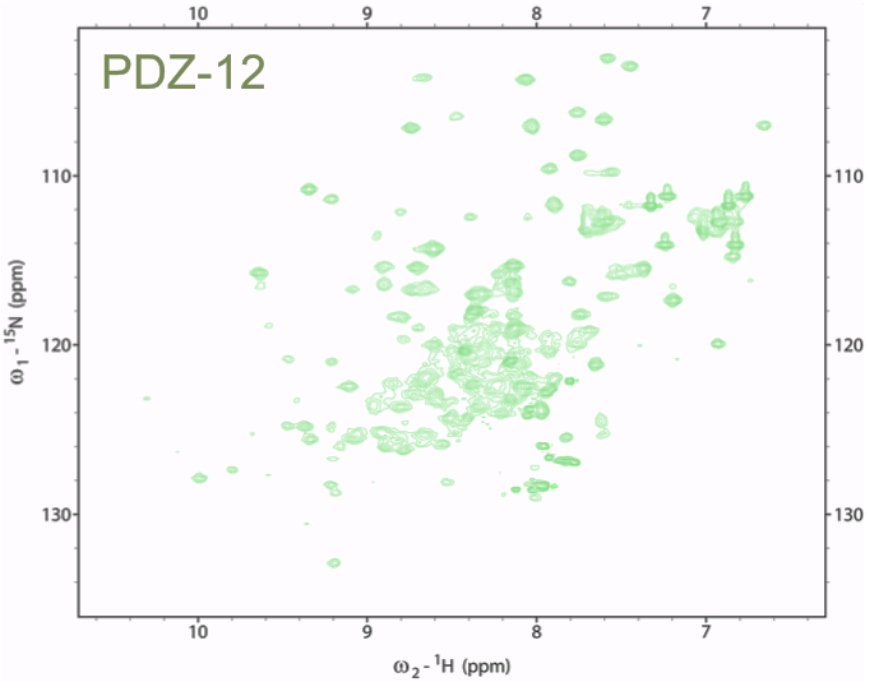

Figure 8: ^{15}N-HSQC of PDZ1+2. Each peak denotes a backbone amide of a non-proline residue or side chains of Asn, Arg, Gln, and Trp.

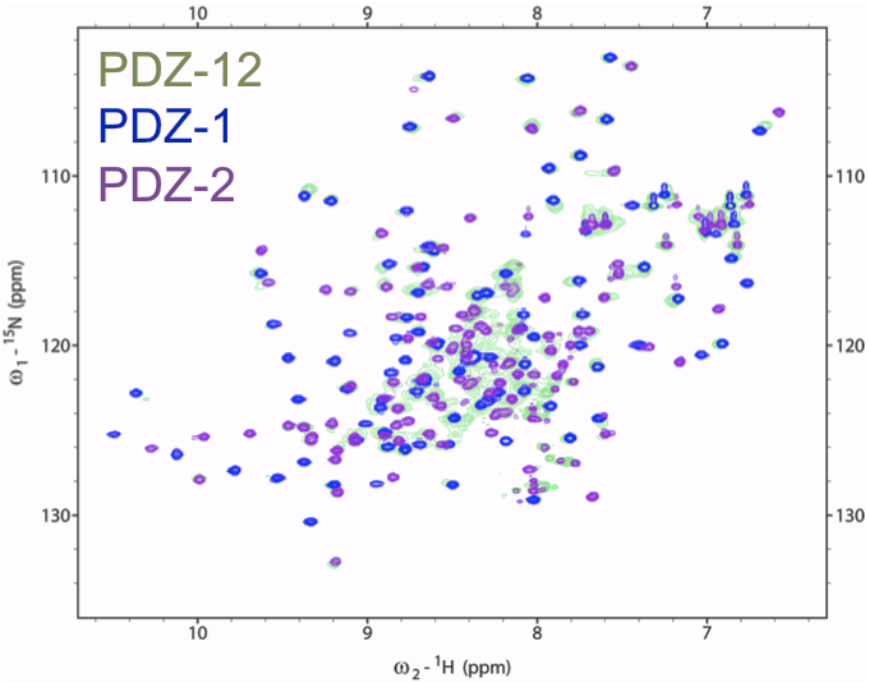

Figure 9: ^{15}N-HSQC overlay of PDZ1 and PDZ2 on PDZ1+2. Each peak denotes a backbone amide of a non-proline residue or side chains of Asn, Arg, Gln, and Trp. Uneven peak intensities indicate inter-domain conformational exchange and interaction between PDZ1 and PDZ2.

A residue specific snapshot of PDZ2+3 structure was obtained by NMR ^{15}N-HSQC spectrum (**Figure 10**). The resonance peaks of PDZ2+3 are monodispersed and well resolved, indicating that it is well folded in solution. Comparison of the HSQC of PDZ2, PDZ3, and PDZ2+3 by overlaying the three shows that there are no significant perturbations in the PDZ2 region, but there are for PDZ3 (**Figure 11**). The specific perturbation in the PDZ3 region indicates that PDZ3, but not PDZ2, interacts with the second inter-domain linker between PDZ2 and PDZ3.

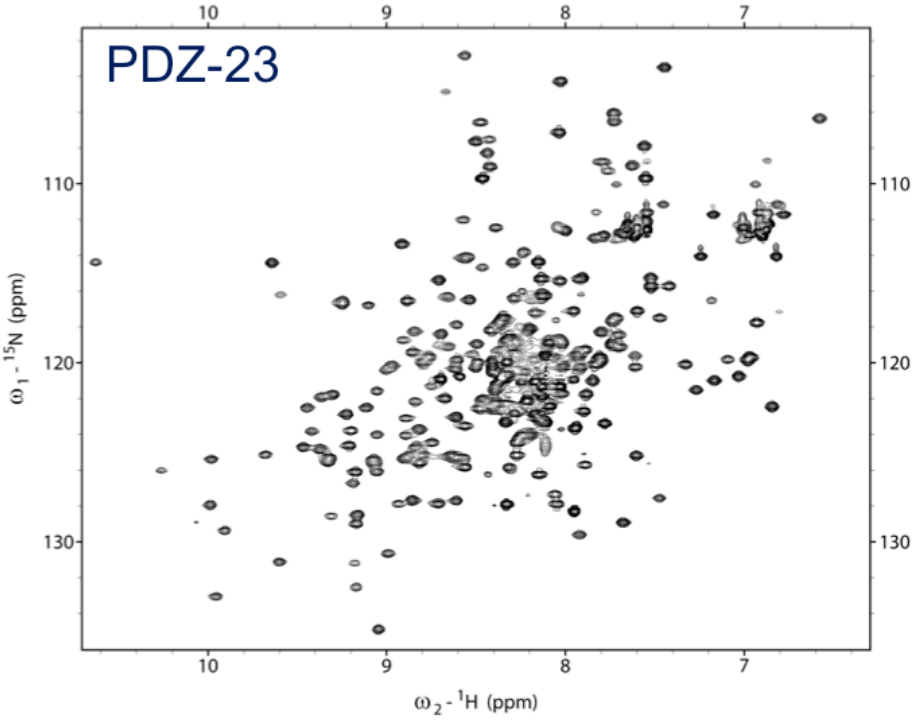

Figure 10: ^{15}N-HSQC of PDZ2+3. Each peak denotes a backbone amide of a non-proline residue or side chains of Asn, Arg, Gln, and Trp.

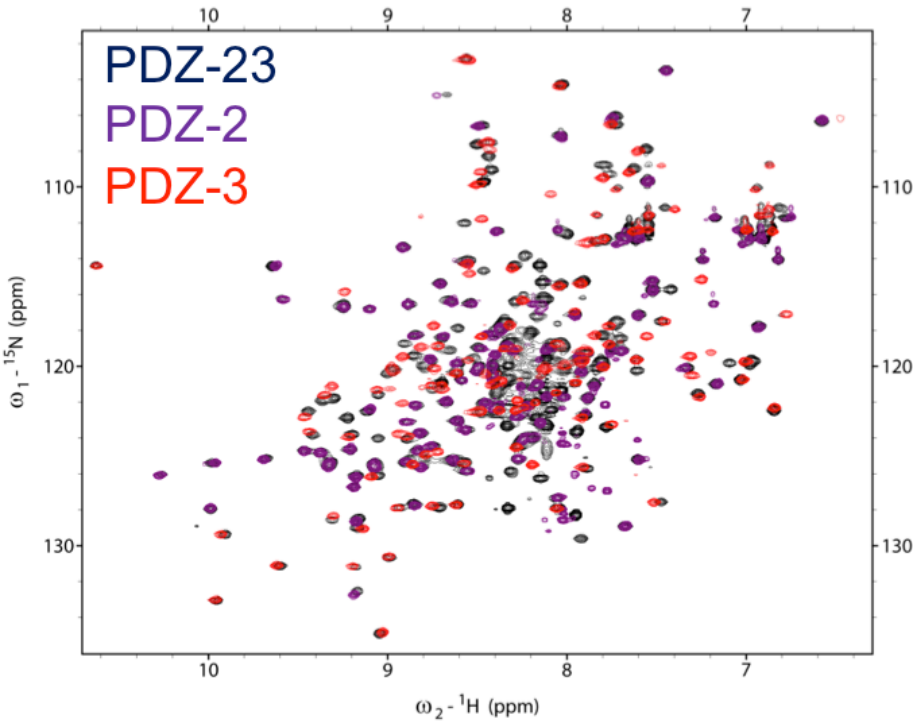

Figure 11: ^{15}N-HSQC overlay of PDZ2 and PDZ3 on PDZ2+3. Each peak denotes a backbone amide of a non-proline residue or side chains of Asn, Arg, Gln, and Trp. Significant perturbations in PDZ3 region indicate interaction with the second inter-domain linker.

A residue specific snapshot of entire tri-domain PDZ region was obtained by NMR ^{15}N-HSQC spectrum (**Figure 12**). The resonance peaks of PDZ1+2+3 are monodispersed, but given that there are over 300 residues, not every individual residue is resolved. Comparison of the HSQC of PDZ1, PDZ2, PDZ3, and PDZ1+2+3 by overlaying the four shows that there are some quaternary interactions between the individual PDZ domains (**Figure 13**). The binding of a drug like CN2097 to one PDZ domain is likely to be affected by these quaternary interactions between the domains.

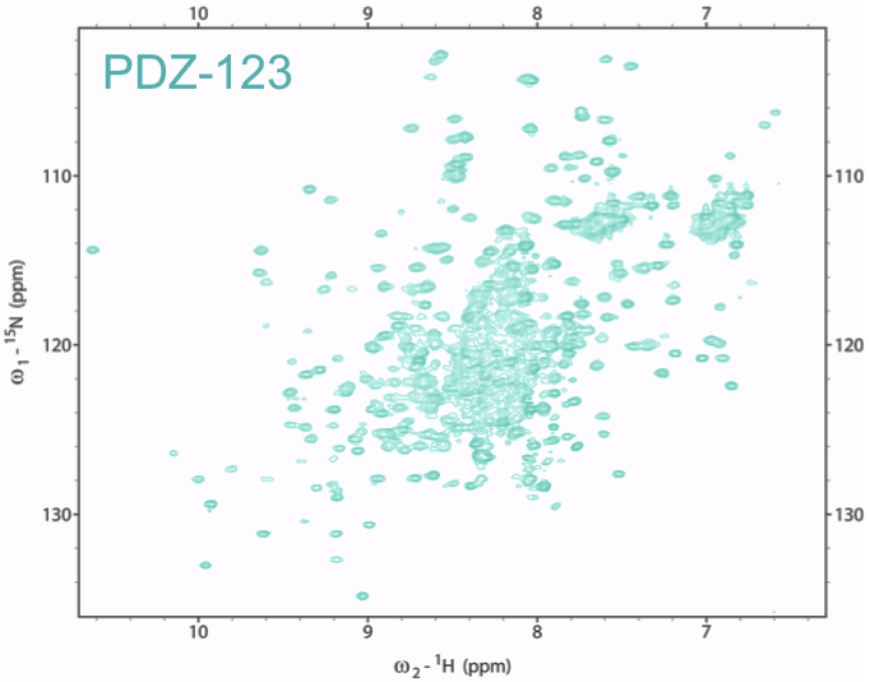

Figure 12: ^{15}N-HSQC of PDZ1+2+3. Each peak denotes a backbone amide of a non-proline residue or side chains of Asn, Arg, Gln, and Trp.

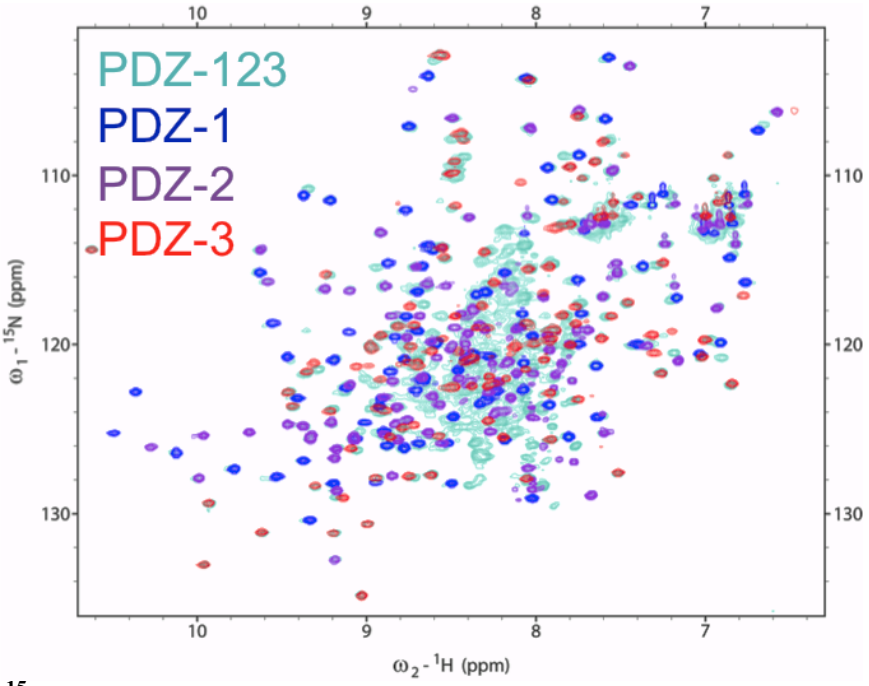

Figure 13: ^{15}N-HSQC overlay of PDZ1, PDZ2, and PDZ3 on PDZ1+2+3. Each peak denotes a backbone amide of a non-proline residue or side chains of Asn, Arg, Gln, and Trp. Significant perturbations in PDZ1+2+3 indicate quaternary interactions among the PDZ domains.

NMR spectroscopy of PDZ/CN2097 interactions

Residue specific snapshots of PDZ1/CN2097 complex and PDZ3/CN2097 complex were obtained by NMR ^{15}N-HSQC spectrum. The overlay of the HSQC of the PDZ3 and PDZ3/CN2097 complex shows significant perturbations in resonance peaks compared to the HSQC overlay of PDZ1 and PDZ1/CN2097 complex (**Figure 14**). The resonance peaks of PDZ1 have shifted after the addition of CN2097, but the peaks of PDZ3 after adding CN2097 shifted even more. This indicates that CN2097 binds to PDZ3 more strongly than to PDZ1. Statistical analysis of the chemical shift perturbations in the backbone amides of PDZ3 on CN2097 binding shows that the binding pocket is located between the second α-helix and second β-sheet, and that the β2-β3 loop is affected (**Figure 15**).

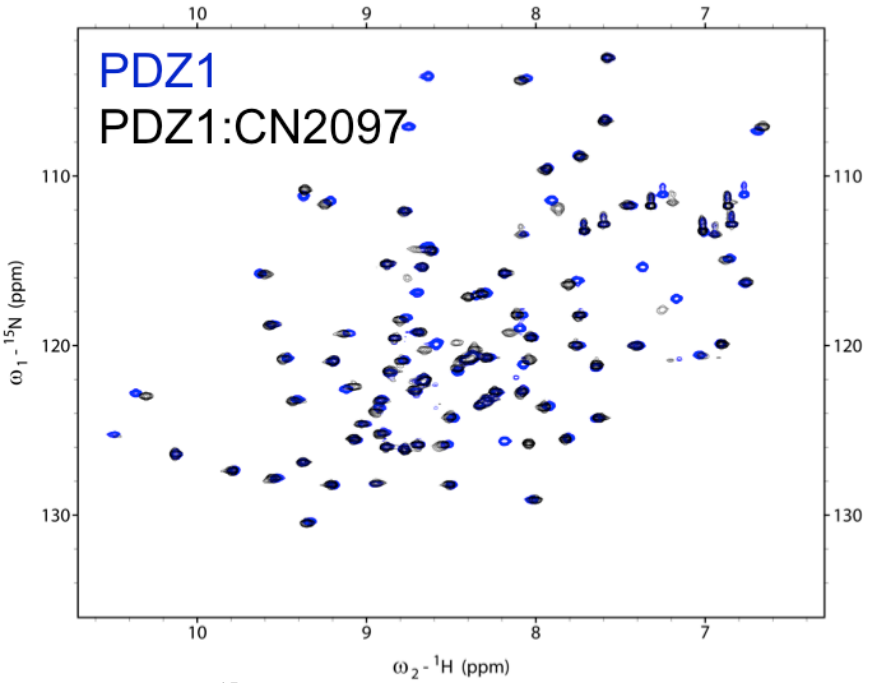

Figure 14: Comparison of ^{15}N-HSQC overlay of PDZ1 and PDZ1/CN2097 complex and ^{15}N-HSQC overlay of PDZ3 and PDZ3/CN2097 complex. Each peak denotes a backbone amide of a non-proline residue or side chains of Asn, Arg, Gln, and Trp.

Greater perturbations in the PDZ3/CN2097 complex indicate stronger binding of CN2097 to PDZ3 than to PDZ1.

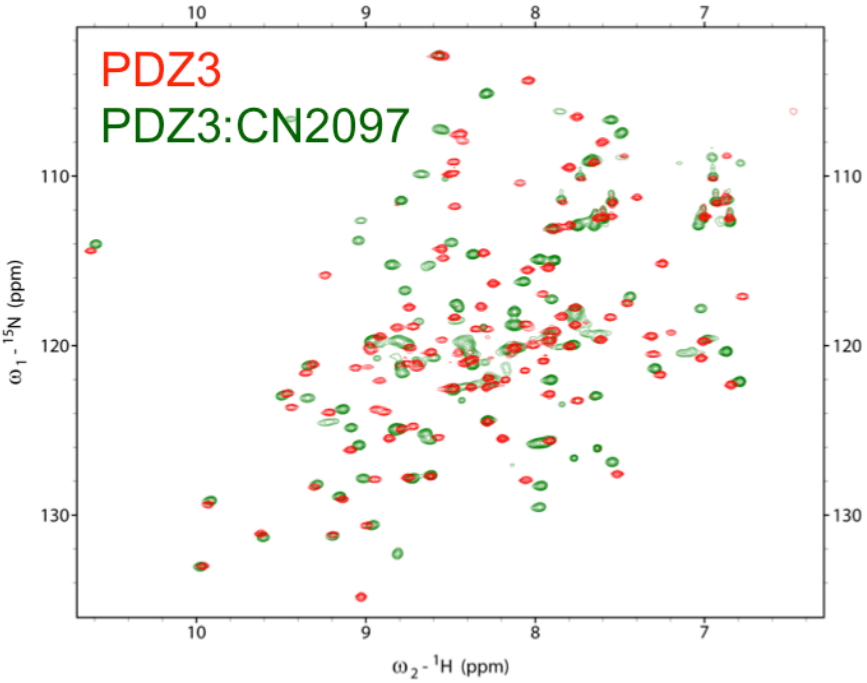

Figure 14 continued: Comparison of ^{15}N-HSQC of overlay of PDZ1 and PDZ1/CN2097 complex and ^{15}N-HSQC overlay of PDZ3 and PDZ3/CN2097 complex. Each peak denotes a backbone amide of a non-proline residue or side chains of Asn, Arg, Gln, and Trp. Greater perturbations in the PDZ3/CN2097 complex indicate stronger binding of CN2097 to PDZ3 than to PDZ1.

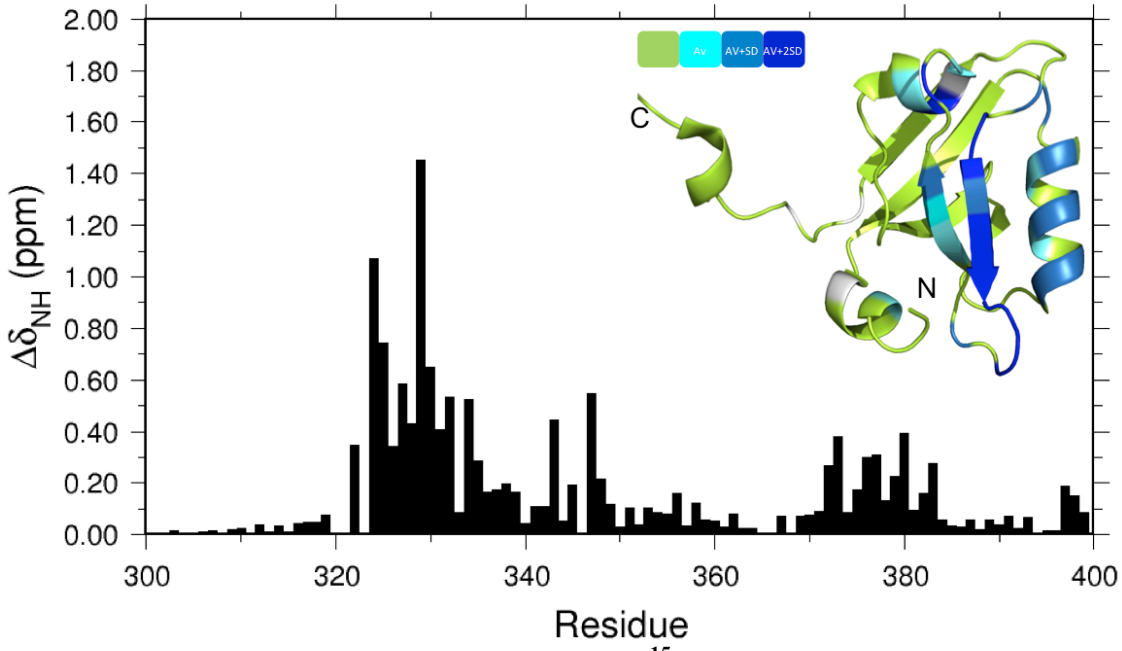

Figure 15. NMR chemical shift perturbations of ^{15}N-PDZ3/unlabeled CN2097 complex. The average chemical shift perturbations in the backbone amides of PDZ3 upon CN2097 binding are shown here. The dark blue represents perturbations of more than two standard deviations from average, the light blue represents perturbation less than two but more than one standard deviation, from average, the cyan represents perturbation less than one standard deviation from average, and the green represents perturbation less than average.

The ^{15}N-HSQC overlay of PDZ1long/CaM complex is monodispersed and well resolved. Overlaying it on the ^{15}N-HSQC of PDZ1long shows significant perturbations in resonance peaks (**Figure 16**). The peaks that are shifted are not only those representing the N-terminal α-helix region but the entire PDZ1long protein. This indicates that the CaM not only binds to the N-terminal α-helix but also interacts with the PDZ1 domain. The binding of CaM to the N-terminal α-helix of PSD-95 has been previously studied (Zhang et al., 2014) using a peptide without the folded PDZ1 domain.

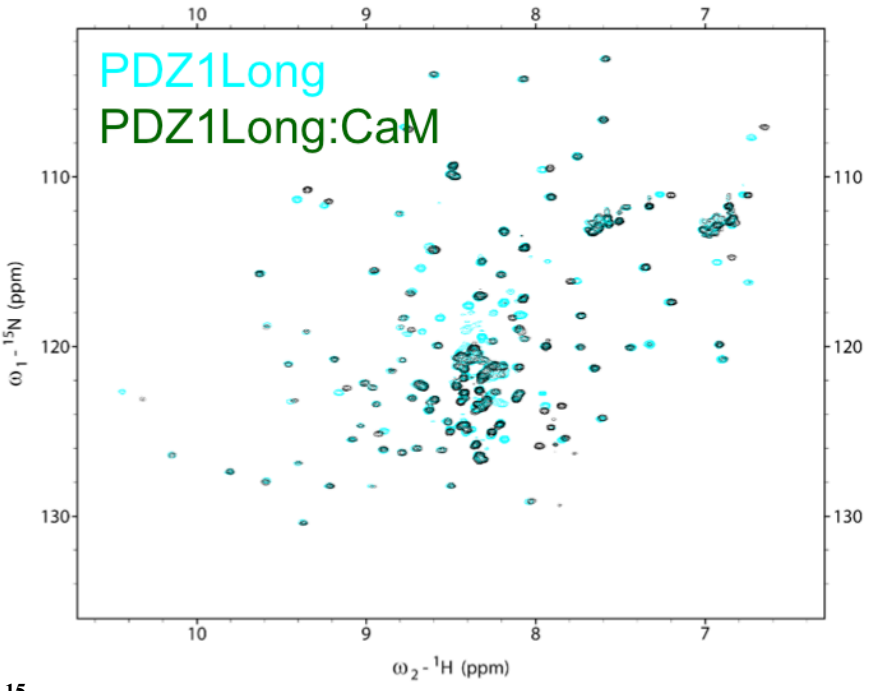

Figure 16: ^{15}N-HSQC overlay of PDZ1long/CaM complex on PDZ1long. Each peak denotes a backbone amide of a non-proline residue or side chains of Asn, Arg, Gln, and Trp. Significant perturbations indicate binding of CaM to the N-terminal α-helix and interaction with PDZ1.

The ^{15}N-HSQC overlay of PDZ1long/CaM complex and PDZ1long/CaM/CN2097 complex shows no significant perturbations in resonance peaks (**Figure 17**). This indicates that CN2097 does not bind to PDZ1 in the presence of CaM.

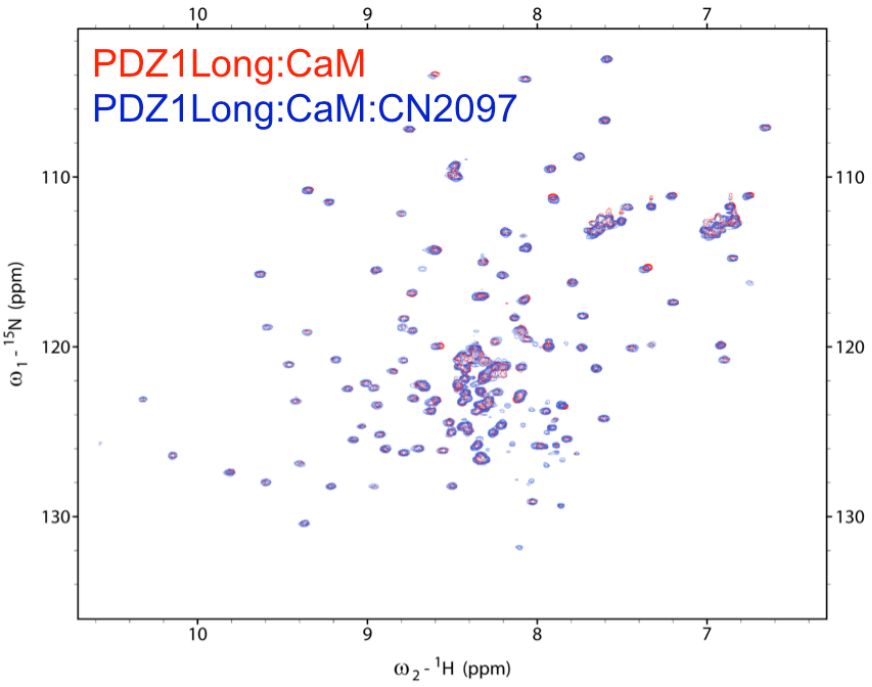

Figure 17: ^{15}N-HSQC overlay of PDZ1long/CaM/CN2097 complex on PDZ1long/CaM complex. Each peak denotes a backbone amide of a non-proline residue or side chains of Asn, Arg, Gln, and Trp. No significant perturbations indicate that CN2097 does not bind PDZ1 in the presence of CaM.

The 3D- HNCA and HCNO experiments were used to perform a triple resonance backbone assignment of PDZ3/CN2097, which are shown in its ^{15}N-HSQC (**Figure 18**). Similarly, CN2097 resonance assignments were obtained using 2D-TOCSY (**Figure 19**). This data was used in software HADDOCK to create a model of complex between the PDZ3/CN2097. It can be clearly seen that the β2-β3 loop is not conserved between PDZ1 and PDZ3 (**Figure 20**).

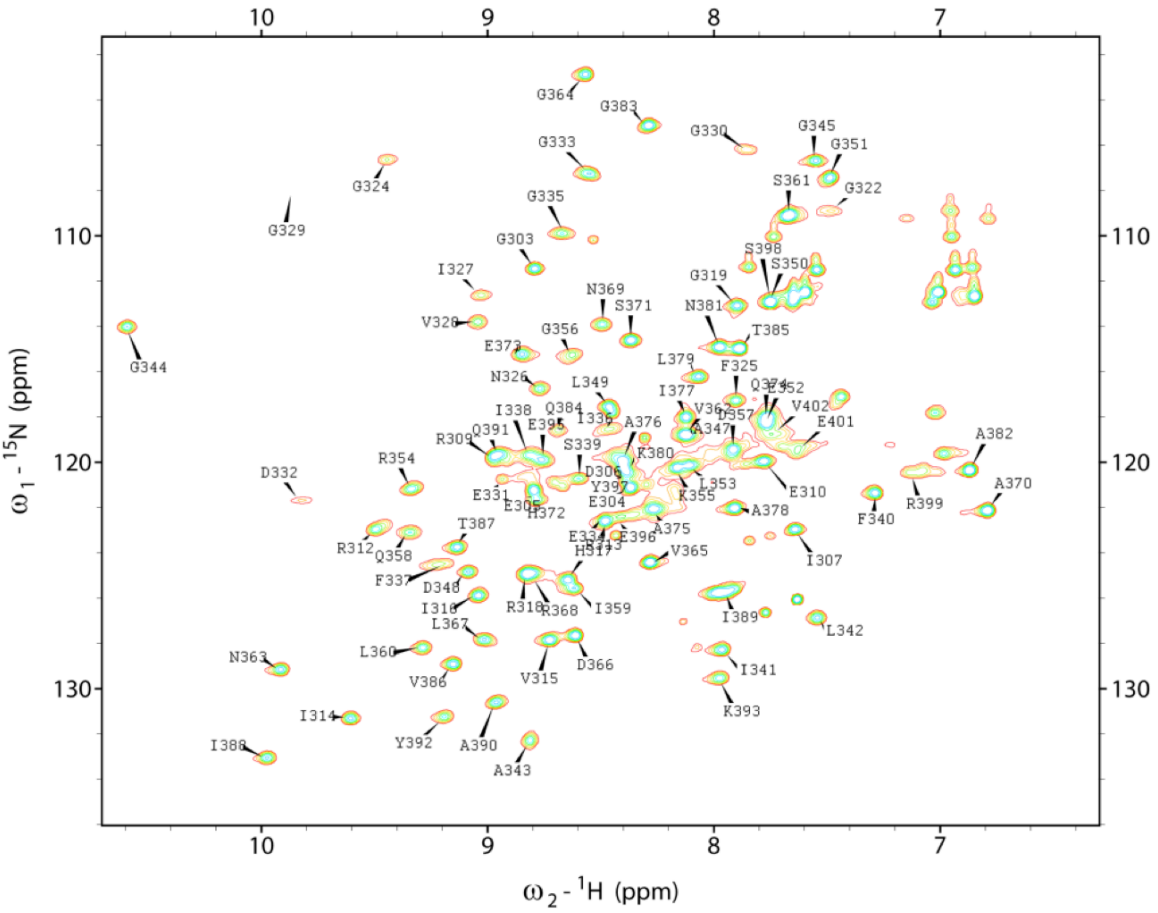

Figure 18: HSQC of ^{15}N-PDZ3/unlabeled CN2097 complex. Each peak denotes a backbone amide of a non-proline residue or side chains of Asn, Arg, Gln, and Trp. The backbone assignment of each residue was made using data acquired from 3D- HNCA experiment.

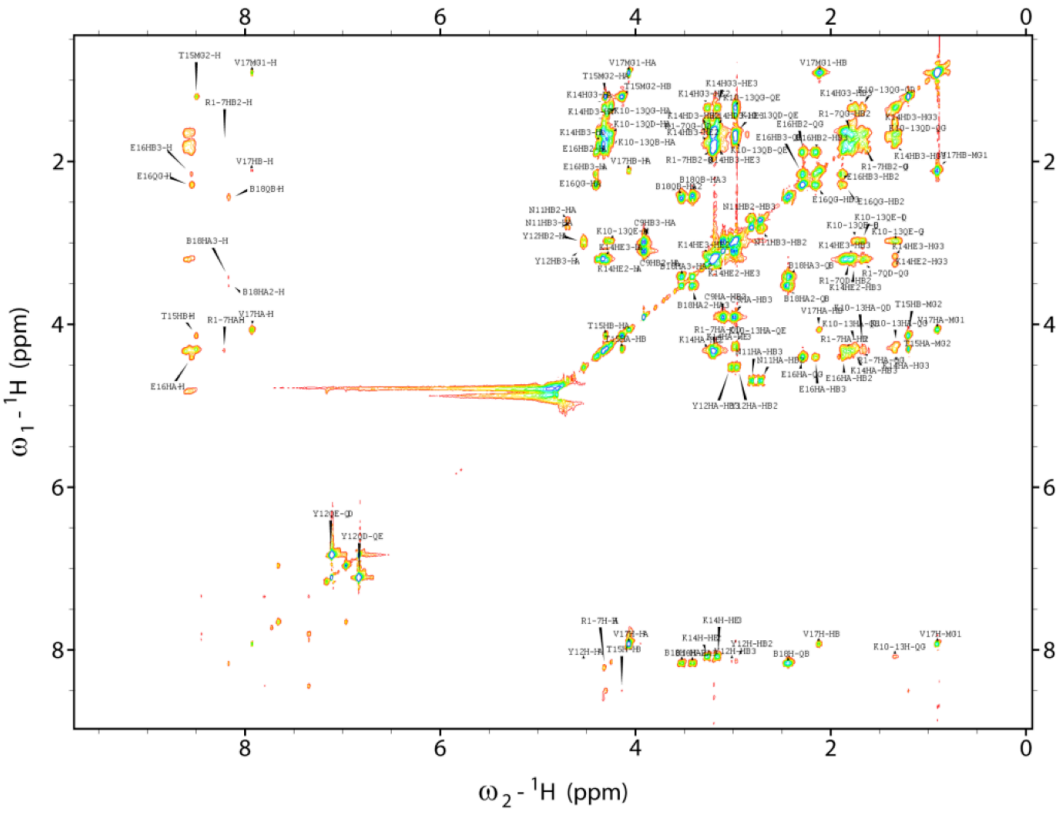

Figure 19: 2D-TOCSY on CN2097.

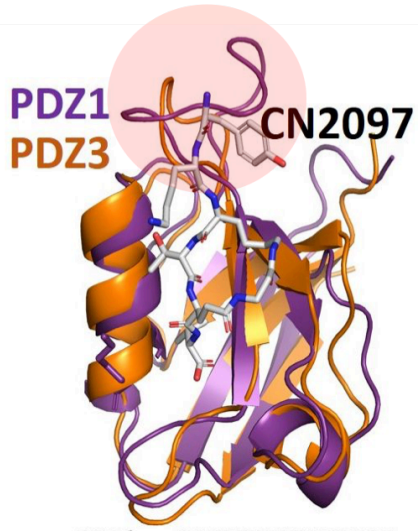

Figure 20: Overlay of structures of PDZ1 and PDZ3. The cyclic peptide portion of CN2097 is shown with sticks.

DISCUSSION

PDZ inter-domain interactions

The ITC data acquired was unreliable in determining binding parameters for PDZ1long, PDZ1, PDZ2, and PDZ1+2. There are no ITC data for a comparison to be made between CN2097 affinities and effect of the inter-domain interactions. If there were inter-domain interactions, ITC results would, in theory, suggest a different binding affinity of PDZ1long, PDZ1+2, and PDZ2+3 to CN2097. However, the ^{15}N-HSQC spectra acquired helped us overcome this problem.

The lack of significant perturbations in PDZ1long compared to PDZ1 indicates that there are no significant contacts between the N-terminal CaM-binding α-helix and the PDZ1 domain (**Figure 7**). Due to the presence of the α-helix, some minor perturbations are bound to be seen, but there are no significant shifts in resonance peaks that would have suggested significant interaction in the N-term helix and PDZ1 domain. The same is true for PDZ2 and the second inter-domain linker. The lack of significant PDZ2+3 perturbations in the PDZ2 region indicates there is no interaction between PDZ2 and the second inter-domain linker. However, there is an interaction between the second inter-domain linker and PDZ3, as evident in NMR spectra (**Figure 11**). This opens up questions on its effect on binding, such as how CN2097 and other ligands will bind PDZ3 when it is part of the entire PSD-95 protein as opposed to an isolated domain. ITC data suggests that the presence of the linker and PDZ2 decrease the binding affinity of CN2097 for the PDZ3 domain (Table 1).

The uneven peak intensities of PDZ1+2 indicate the presence of inter-domain conformational exchanges and interaction between PDZ1 and PDZ2 (**Figure 9**). The peaks do not overlap perfectly, and this might be due to the fact that the inter-domain linker between the PDZ1 and PDZ2 is only nine residues long, causing the two domains to be close in proximity and thus undergo conformational exchange. This raises questions such as how they interact and to what extent does it have any effect on how drugs like CN2097 and other ligands bind.

PDZ and drug interactions

The ITC data would have provided the binding parameters of CN2097 binding to the isolated domains. In theory, if the dissociation constant of PDZ1 were smaller than PDZ1long, then that would indicate the N-terminal α-helix interferes with ligand binding. Likewise, if the dissociation constant of PDZ1 and PDZ2 were each smaller than PDZ1+2, then that would also indicate that the binding of CN2097 is affected by protein interactions from the other PDZ domains.

CN2097 binding to PDZ3 is tighter when it is isolated than when PDZ2 and the second inter-domain linker are present. This suggests that there is something interfering with the binding of CN2097 to PDZ3. The ITC data both support this, as the dissociation constant of PDZ3 was smaller than that of PDZ2+3. The NMR data also supports this, as the PDZ3 region of PDZ2+3 is significantly perturbed. CN2097 also appears to bind to PDZ3 more tightly than to PDZ1. The binding pocket of PDZ3 is located similarly to PDZ1, between the second α-helix and second β-sheet. Also similarly, the β2-β3 loop is

shown to be affected by ligand association. What is different is that the loop is much shorter in PDZ3, which may be the reason why CN2097 binding perturbs PDZ3 more strongly than PDZ1. CN2097 also does not appear to bind to PDZ1long in the presence of CaM. The implication of this being, *in vivo* where CaM is abundant and the PDZ domains are part of the entire PSD-95 protein, CaM will bind to the N-terminal α-helix and interfere with the binding of CN2097 to PDZ1, causing it to preferably bind PDZ3.

Limitations of ITC and NMR

ITC is limited by its need for relatively high concentrations of protein and ligand. The proteins of interest were not always expressed at the concentration that was necessary for a successful experiment, which was typical ~100μM. To achieve a high enough concentration, the protein often required concentrating, risking precipitation. The need for the ligand to be 10-15x the protein concentration was also a challenge, requiring milligrams quantities of CN2097 to meet the 1mM concentration needed when only milligrams were available. Measurement times are relatively long and the reagents cannot be reused.

NMR spectroscopy poses a similar limitation, requiring hundreds of microliters of samples at similar protein concentrations. Proteins need to be below a certain size to be useful for NMR studies. The proteins used in this study were soluble and small enough to be well resolved, although PDZ1+2+3 was rather large at ~40kDa. Another limitation is the relatively low sensitivity in comparison to other techniques such as mass

spectrometry. The advantage of NMR to mass spectrometry, however, is that NMR can provide information on the folded state of proteins.

Future research implications

In this study, inter-domain interactions between PDZ domains were identified and the NMR resonance assignment of PDZ3/CN2097 complex was completed. Both of these findings allow for the future development of CN2097 on two fronts. One is research towards reducing proteolysis and the other is to improve the drug's binding affinity. The CRIPT peptide that the cyclic peptide of CN2097 was based on was found to bind to PDZ3, yet the drug has been developed to bind to PDZ1. Knowing that inter-domain interactions exist and may interfere with drug binding, as well as the likelihood of CaM limiting drug binding *in vivo*, it will be interesting to further investigate what effects those interactions will have on drug binding. The effects of those interactions may have further implications on how the drug can be further developed.

REFERENCES

Aarts, M., Liu, Y., Liu, L., Besshoh, S., Arundine, M., Gurd, J. W., … Tymianski, M. (2002). Treatment of Ischemic Brain Damage by Perturbing NMDA Receptor- PSD-95 Protein Interactions. *Science*, *298*(5594), 846–850. https://doi.org/10.1126/science.1072873

Bats, C., Groc, L., & Choquet, D. (2007). The Interaction between Stargazin and PSD-95 Regulates AMPA Receptor Surface Trafficking. *Neuron*, *53*(5), 719–734. https://doi.org/10.1016/j.neuron.2007.01.030

Bliss, T. V. P., Collingridge, G. L., & Morris, R. G. M. (2014). Synaptic plasticity in health and disease: introduction and overview. *Philosophical Transactions of the Royal Society B: Biological Sciences*, *369*(1633). https://doi.org/10.1098/rstb.2013.0129

Boeckers, T. M. (2006). The postsynaptic density. *Cell and Tissue Research*, *326*(2), 409–422. https://doi.org/10.1007/s00441-006-0274-5

Cao, C., Rioult-Pedotti, M. S., Migani, P., Yu, C. J., Tiwari, R., Parang, K., … Marshall, J. (2013). Impairment of TrkB-PSD-95 Signaling in Angelman Syndrome. *PLOS Biology*, *11*(2), e1001478. https://doi.org/10.1371/journal.pbio.1001478

Colledge, M., Snyder, E. M., Crozier, R. A., Soderling, J. A., Jin, Y., Langeberg, L. K., … Scott, J. D. (2003). Ubiquitination Regulates PSD-95 Degradation and AMPA Receptor Surface Expression. *Neuron*, *40*(3), 595–607. https://doi.org/10.1016/S0896-6273(03)00687-1

Davis, S. M., Lees, K. R., Albers, G. W., Diener, H. C., Markabi, S., Karlsson, G., & Norris, J. (2000). Selfotel in Acute Ischemic Stroke: Possible Neurotoxic Effects of an NMDA Antagonist. *Stroke*, *31*(2), 347–354. https://doi.org/10.1161/01.STR.31.2.347

Doucleff, M., Hatcher-Skeers, M., & Crane, N. J. (2011). *Pocket Guide to Biomolecular NMR* (1st ed.). Springer-Verlag Berlin Heidelberg.

Doyle, D. A., Lee, A., Lewis, J., Kim, E., Sheng, M., & MacKinnon, R. (1996). Crystal Structures of a Complexed and Peptide-Free Membrane Protein–Binding Domain: Molecular Basis of Peptide Recognition by PDZ. *Cell*, *85*(7), 1067–1076. https://doi.org/10.1016/S0092-8674(00)81307-0

Fix, A. S., Horn, J. W., Wightman, K. A., Johnson, C. A., Long, G. G., Storts, R. W., … Olney, J. W. (1993). Neuronal Vacuolization and Necrosis Induced by the Noncompetitive N-methyl-d-aspartate (NMDA) Antagonist MK(+)801 (Dizocilpine

Maleate): A Light and Electron Microscopic Evaluation of the Rat Retrosplenial Cortex. *Experimental Neurology*, *123*(2), 204–215. https://doi.org/10.1006/exnr.1993.1153

French, J. A., Krauss, G. L., Steinhoff, B. J., Squillacote, D., Yang, H., Kumar, D., & Laurenza, A. (2013). Evaluation of adjunctive perampanel in patients with refractory partial-onset seizures: Results of randomized global phase III study 305. *Epilepsia*, *54*(1), 117–125. https://doi.org/10.1111/j.1528-1167.2012.03638.x

Fritsch, B., Reis, J., Gasior, M., Kaminski, R. M., & Rogawski, M. A. (2014). Role of GluK1 Kainate Receptors in Seizures, Epileptic Discharges, and Epileptogenesis. *The Journal of Neuroscience*, *34*(17), 5765–5775. https://doi.org/10.1523/JNEUROSCI.5307-13.2014

Fukata, Y., Dimitrov, A., Boncompain, G., Vielemeyer, O., Perez, F., & Fukata, M. (2013). Local palmitoylation cycles define activity-regulated postsynaptic subdomains. *The Journal of Cell Biology*, *202*(1), 145–161. https://doi.org/10.1083/jcb.201302071

Fukunaga, Y., Matsubara, M., Nagai, R., & Miyazawa, A. (2005). The Interaction between PSD-95 and Ca2+/Calmodulin Is Enhanced by PDZ-Binding Proteins. *The Journal of Biochemistry*, *138*(2), 177–182. https://doi.org/10.1093/jb/mvi107

Garcia, E. P., Mehta, S., Blair, L. A. C., Wells, D. G., Shang, J., Fukushima, T., … Marshall, J. (1998). SAP90 Binds and Clusters Kainate Receptors Causing Incomplete Desensitization. *Neuron*, *21*(4), 727–739. https://doi.org/10.1016/S0896-6273(00)80590-5

Kay, L. E., Ikura, M., Tschudin, R., & Bax, A. (1990). Three-dimensional triple-resonance NMR spectroscopy of isotopically enriched proteins. *Journal of Magnetic Resonance (1969)*, *89*(3), 496–514. https://doi.org/10.1016/0022-2364(90)90333-5

Kim, E., & Sheng, M. (2004). PDZ domain proteins of synapses. *Nature Reviews Neuroscience*, *5*, 771.

LeBlanc, B. W., Iwata, M., Mallon, A. P., Rupasinghe, C. N., Goebel, D. J., Marshall, J., … Saab, C. Y. (2010). A cyclic peptide targeted against PSD-95 blocks central sensitization and attenuates thermal hyperalgesia. *Neuroscience*, *167*(2), 490–500. https://doi.org/10.1016/j.neuroscience.2010.02.031

Lee, H.-J., & Zheng, J. J. (2010). PDZ domains and their binding partners: structure, specificity, and modification. *Cell Communication and Signaling : CCS*, *8*, 8. https://doi.org/10.1186/1478-811X-8-8

Lerma, J., & Marques, J. M. (2013). Kainate Receptors in Health and Disease. *Neuron*, *80*(2), 292–311. https://doi.org/10.1016/j.neuron.2013.09.045

Li, T., Saro, D., & Spaller, M. R. (2004). Thermodynamic profiling of conformationally constrained cyclic ligands for the PDZ domain. *Bioorganic & Medicinal Chemistry Letters*, *14*(6), 1385–1388. https://doi.org/10.1016/j.bmcl.2003.09.103

Liang, Y. (2008). Applications of isothermal titration calorimetry in protein science. *Acta Biochimica et Biophysica Sinica*, *40*(7), 565–576. https://doi.org/10.1111/j.1745-7270.2008.00437.x

Marshall, J., Szmydynger-Chodobska, J., Rioult-Pedotti, M. S., Lau, K., Chin, A. T., Kotla, S. K. R., … Chodobski, A. (2017). TrkB-enhancer facilitates functional recovery after traumatic brain injury. *Scientific Reports*, *7*(1), 10995. https://doi.org/10.1038/s41598-017-11316-8

Paarmann, I., Spangenberg, O., Lavie, A., & Konrad, M. (2002). Formation of Complexes between Ca2+·Calmodulin and the Synapse-associated Protein SAP97 Requires the SH3 Domain-Guanylate Kinase Domain-connecting HOOK Region. *Journal of Biological Chemistry*, *277*(43), 40832–40838. https://doi.org/10.1074/jbc.M205618200

Piserchio, A., Pellegrini, M., Mehta, S., Blackman, S. M., Garcia, E. P., Marshall, J., & Mierke, D. F. (2002). The PDZ1 Domain of SAP90 CHARACTERIZATION OF STRUCTURE AND BINDING. *Journal of Biological Chemistry*, *277*(9), 6967–6973. https://doi.org/10.1074/jbc.M109453200

Piserchio, A., Salinas, G. D., Li, T., Marshall, J., Spaller, M. R., & Mierke, D. F. (2004). Targeting Specific PDZ Domains of PSD-95: Structural Basis for Enhanced Affinity and Enzymatic Stability of a Cyclic Peptide. *Chemistry & Biology*, *11*(4), 469–473. https://doi.org/10.1016/j.chembiol.2004.03.013

Ponting, C. P. (1997). Evidence for PDZ domains in bacteria, yeast, and plants. *Protein Science : A Publication of the Protein Society*, *6*(2), 464–468.

Rogawski, M. A. (2013). AMPA Receptors as a Molecular Target in Epilepsy Therapy. *Acta Neurologica Scandinavica. Supplementum*, (197), 9–18. https://doi.org/10.1111/ane.12099

Sornarajah, L., Vasuta, O. C., Zhang, L., Sutton, C., Li, B., El-Husseini, A., & Raymond, L. A. (2008). NMDA receptor desensitization regulated by direct binding to PDZ1-2 domains of PSD-95. *Journal of Neurophysiology*, *99*(6), 3052–3062. https://doi.org/10.1152/jn.90301.2008

Suzuki, E., & Kamiya, H. (2016). PSD-95 regulates synaptic kainate receptors at mouse hippocampal mossy fiber-CA3 synapses. *Neuroscience Research*, *107*, 14–19. https://doi.org/10.1016/j.neures.2015.12.011

Tochio, H., Hung, F., Li, M., Bredt, D. S., & Zhang, M. (2000). Solution structure and backbone dynamics of the second PDZ domain of postsynaptic density-9511Edited by P. E. Wright. *Journal of Molecular Biology*, *295*(2), 225–237. https://doi.org/10.1006/jmbi.1999.3350

Velazquez-Campoy, A., Leavitt, S. A., & Freire, E. (2004). Characterization of Protein-Protein Interactions by Isothermal Titration Calorimetry. In H. Fu (Ed.), *Protein-Protein Interactions: Methods and Applications* (pp. 35–54). Totowa, NJ: Humana Press. https://doi.org/10.1385/1-59259-762-9:035

Zhang, Y., Matt, L., Patriarchi, T., Malik, Z. A., Chowdhury, D., Park, D. K., … Hell, J. W. (2014). Capping of the N-terminus of PSD-95 by calmodulin triggers its postsynaptic release. *The EMBO Journal*, *33*(12), 1341–1353. https://doi.org/10.1002/embj.201488126

CURRICULUM VITAE